SIMULATION OF THE CHARGE RATIO OF COSMIC RAY MUONS IN EXTENSIVE AIR SHOWERS USING CORSIKA

BY

OCHILO LIVINGSTONE ONYANGO [B.Ed (Sc)]
REGISTRATION NUMBER I56/10290/2006

A thesis submitted in partial fulfillment of the requirements for the award of the degree of Master of Science in the school of Pure and Applied Sciences of Kenyatta University

August 2010

DECLARATION

This thesis is my original work and has not been presented for a degree in any other university or any other award.

Signature _____ Date 5.10.2010

Ochilo, Livingstone Onyango
Department of Physics
Kenyatta University

We confirm that the work reported in this thesis was carried out by the candidate under our supervision.

Signature _____ Date 05.10.2010

Dr. N.O. Hashim
Department of Physics
Kenyatta University

Signature _____ Date 5.10.2010

Prof. J. Okumu
Department of Physics
Kenyatta University

DEDICATION

This thesis is dedicated to my wife Sarah, and to my sons Marvel, Joe and Kevin.

ACKNOWLEDGEMENT

I would like to acknowledge the guidance and encouragement given to me from the beginning of this work through to the end by my supervisors Dr. Hashim and Prof. Okumu. I am particularly grateful for their constant availability for consultation, even when they were pressed with other responsibilities. I acknowledge with gratitude Dr Hashim for availing to me the graph of the all-particle cosmic ray spectrum (fig. 3.1) and the data from the CosmoALEPH collaboration for comparison with the simulated data.

I am grateful to my employer, the teachers service commission, for granting me study leave, which enabled me to fully concentrate on my studies.

I also wish to thank my classmates, including Mr. Jobunga, Mr. Mugambi, Mr. Zavani, Mr. Kebwaro, Mr. Okiambe and Mr. Agumba for being always there for mutual encouragement and consultation all through this study.

My family has been a constant source of motivation and inspiration for me during this study. I thank my wife Sarah, and my sons Marvel, Joe and Kevin for their patience during the long periods of my absence from home in the course of this study. I am greatly indebted to my late parents who sacrificed so much, to ensure that I go to school.

Above all, I thank the almighty God for His protection, and provision of good health and all that I needed for this study. All the glory to Him.

TABLE OF CONTENTS

LIST OF FIGURES

LIST OF TABLES

ABBREVIATIONS AND ACRONYMS

ALEPH	Apparatus for Large Electron Positron collider PHysics.
CORSIKA	Cosmic Ray Simulations for KAscade.
DPMJET	Dual Parton Model with JETs.
EAS	Extensive Air Shower
EGS4	Electron Gamma Shower version 4
GHEISHA	Gamma Hadron Electron Interaction SHower code
KASCADE	KArlsruhe Shower Core Array Detector
MINOS	Main Injector Neutrino Oscillation Search
NEXUS	NEXt generation of Unified Scattering approach
NKG	Nishimura-Kamata-Greisen formula
QGSJET	Quark Gluon String model with JETs
VENUS	Very Energetic NUclear Scattering
WILLI	Weakly Ionizing Lepton Lead Interactions

ABSTRACT

The interaction of primary cosmic rays in the atmosphere produces, among other particles, pions and kaons. They decay to muons, which form an important component of extensive air showers, which can be measured on the Earth's surface. The ratio of positively to negatively charged muons, called the muon charge ratio, provides important information about the cosmic ray interactions in the atmosphere. In this study, the theoretical hadronic interaction models in the cosmic ray simulation code CORSIKA are used to study the charge ratio of cosmic ray muons simulated in extensive air showers. An East – West effect on the charge ratio of simulated cosmic ray muons is observed. It is more pronounced for inclined and low-energy muons (momentum less than 100 GeV/c and zenith angle greater than 80°). Experimental data from MINOS Near and WILLI experiments give similar results.

1 INTRODUCTION

1.1 Background

Cosmic radiation was first measured in 1911 by Victor Hess. Using a balloon-borne pressurized ionization chamber, Hess observed that the rate of ionization at an altitude of 5 km was several times higher than that observed at sea level. Other subsequent experiments and mathematical analyses done using more refined techniques established the nature of cosmic rays (Hayakawa, 1969). Cosmic rays may be classified into primary and secondary cosmic rays. Particles and radiation from outside the Earth's atmosphere, which arrive unperturbed at the Earth's atmosphere, are called primary cosmic rays. The primary cosmic rays consist of charged particles, mainly protons ($\approx$85%) and α -particles ($\approx$12%). Elements with a nuclear charge $Z \geq 3$ make up 3% of charged primary cosmic rays. Neutral particles of cosmic rays consist of γ-rays, neutrinos and antineutrinos. The bulk of the primary radiation is of galactic origin (Grupen, 2005).

The interaction of primary cosmic rays with atomic nuclei in the atmosphere results in the production of secondary cosmic rays. The interaction of a proton in the atmosphere is illustrated in figure 1.1. Secondary cosmic rays consist of various components, which are defined depending on, among other factors, the method of observation. The component that is rapidly absorbed in the Earth's atmosphere is called the soft component. It is attributed mainly to electrons. The hard component is attributed to heavier particles, which do not undergo bremsstrahlung.

An interaction of the primary cosmic rays incident on the Earth's atmosphere from outer space with atmospheric nuclei often results in the generation of a shower that consists of a bundle of particles. The first kind of a shower, associated with the soft component, is accounted for in terms of the cascade shower of electrons and photons. Hence the particles of such showers are collectively called the *electronic component* or *E-*

component. In the second kind of shower, both the primary and secondary particles consist of nucleons and charged pions, which form the *nuclear active component (N-component).* The electronic and hadronic cascades not only develop longitudinally, but also spread out laterally in the atmosphere.

The extent of lateral spreading is determined by the multiple scattering of electrons and positrons in the electromagnetic cascades. In hadronic cascades, it is determined by the transverse momenta at the production of secondary particles. A larger transverse momentum leads to a larger lateral width of the shower. Both the longitudinal and lateral development of an extensive air shower are influenced by the type of primary particle and its energy. For example, iron nuclei interact earlier in the atmosphere than protons of the same energy. The lateral width of an iron shower is also greater. However, at sea level, most cosmic ray particles do not belong to either the electromagnetic or hadronic components, but form the penetrating component which comprises mostly of muons (Hayakawa, 1969).

Primary cosmic rays with energies known to exceed 10^{20} eV have been observed. These so-called ultra-high energy cosmic rays (UHECRs), which are strongly interacting particles, have not been well understood since their flux is very low and only limited experimental statistics have been collected (Engel, 2002). At energies beyond 10^{20} eV, the cosmic ray intensity does not exceed 0.5 particles/km^2/sr per century (Sommers, 2004) .

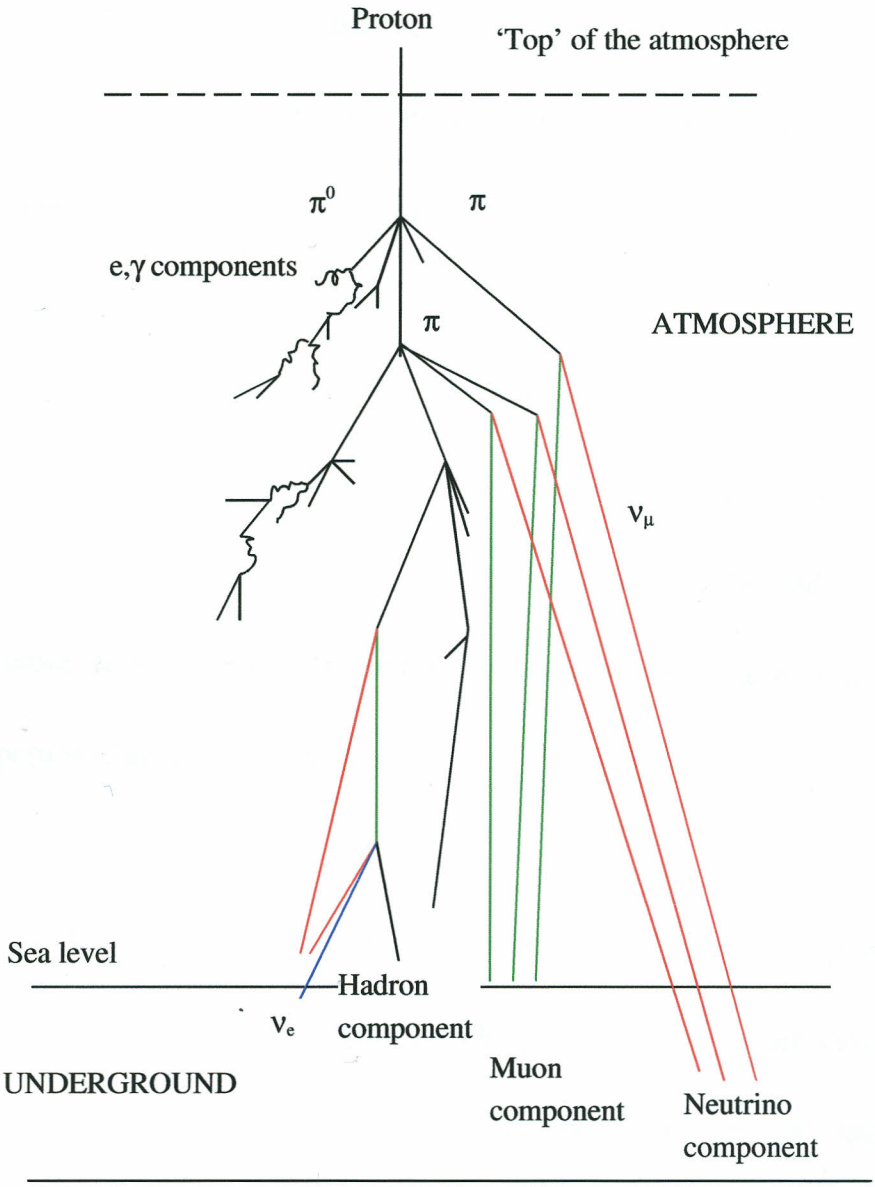

Fig. 1.1 A sketch illustrating the interaction of primary cosmic rays in the atmosphere leading to the production of secondary cosmic rays.

However, the very low flux at these energies makes their measurement difficult. The study of extensive air showers of the highest energies is complicated by the fact that the atmosphere is a part of the detector and the interpretation of measurements is indirect (Cazon *et al.*, 2004).

The air shower is a complex chain of interactions resulting in a large number of particles from which only sparse data samples are taken. From this sample, the properties of the primary particle must be deduced. We therefore have to rely on complex numerical simulations to infer these properties (Cazon *et al.*, 2004).

The muon charge ratio, which is the ratio of the number of positively charged to the number of negatively charged muons in an air shower, is important in giving information about the properties of hadronic interactions. It provides important information on the interactions of the primary cosmic rays with nuclei in the atmosphere (Bahmanabadi *et*

al.,2005). Further more, the charge ratio has been quoted with a relatively high accuracy of ± 5% (Velpascu *et al.*, 1999). This brings about the possibility of an increased accuracy in the analysis of hadronic interactions.

1.2 Statement of the Research Problem

In the recent past, measurements of the charge ratio of atmospheric muons have been made. The CosmoALEPH collaboration used the ALEPH detector at the European Center for Particle Physics, CERN, to measure the charge ratio of cosmic ray muons (Hashim, 2007). A constant, energy-independent value of 1.278 averaged over the momentum range 80 GeV/c to 1 TeV/c was found (Grupen *et al.*, 2008). Although the flux and energy spectra of positive and negative muons have been studied on the basis of Monte Carlo simulations of extensive air showers using CORSIKA, updated versions of CORSIKA have since come into use. Improvements made in the updated versions of CORSIKA code include more accurate description of the interaction cross-sections, taking into account revised parton

distributions (Heck *et al.*,1998). The simulations have intrinsic and unavoidable uncertainties arising from interaction models that require untested extrapolations of low energy accelerator data.

1.3 Hypothesis

The value of the muon charge ratio at low primary energy as revealed by experimental measurements of cosmic rays particle spectra in extensive air showers agrees with that obtained in simulations using hadronic interaction models contained in the updated version of CORSIKA.

1.4 Objectives

1.4.1 Main Objective

To simulate cosmic ray events, determine the muon charge ratio of the muonic component of extensive air showers and compare the results with experimental data.

1.4.2 Specific Objectives

The specific objectives of the research were to:

(i) Track propagating cosmic ray particles from one interaction point to another by performing Monte Carlo simulations.

(ii) Compile the final space, time and momentum coordinates of propagating cosmic ray particles, as well as their energy at the last observation level.

(iii) Compile the charge ratio of muons at selected zenith angles.

(iv) Compare the results with those obtained using experimental data.

1.5 Rationale

Monte Carlo simulations use specific models of hadronic interactions as generators. The models are reflected by the energy-weighted moments. Therefore measurements of the charge ratio are a source of information about the validity of such hadronic interaction models. The simulations

carried out in this research provide a means of testing the updated models for high-energy interactions such as QGSJET II and SIBYLL which have been included in the current version of CORSIKA. Experimental information about charge ratio is very useful in tuning the ingredients of models used for calculations of atmospheric neutrino fluxes.

2 LITERATURE REVIEW

2.1 Muon Charge Ratio and the East-West Effect

An experimentally determined value of the charge ratio of atmospheric muons provides a sensitive test of the simulation models used to predict the fluxes of muons in extensive air showers. The trajectories of both primary and secondary cosmic rays at low energy ($E \leq 100$ GeV) are influenced by the geomagnetic field and also by the magnetic rigidity cut-off of primary cosmic rays penetrating the Earth's atmosphere. This affects the value of the muon charge ratio at low energy. The WILLI detector was used to determine the muon charge ratio for two different locations with different magnetic cut-off: Hiroshima (34°N, 132°E) and Bucharest (44°N, 26°E) for a range of energies below 1 GeV (Brancus *et al.*, 2003; Mitrica *et al.*, 2006). A comparison of the muon charge ratio data for vertical muons and for data measured separately in the East and West directions for muons of inclined incidence (mean angle of incidence 35°) displayed good agreement with data obtained using the WILLI detector. The simulation results

obtained using the GHEISHA model (Fesefeldt *et al.*, 1985) were found to be different from experimental observations. The DPMJET (Ranft, 1999) results agreed generally well with the data from the WILLI detector (Mitrica *et al.*, 2006). The CORSIKA results, obtained using the DPMJET model, were found to agree with the muon charge ratio data and the pronounced East-West effect observed by the WILLI experiment.

The WILLI detector, which is mounted on rotatable frame, measured the muon charge ratio by determining the effective lifetime of stopped muons. The results showed an asymmetry of muon charge ratio, decreasing from 0.25 to 0.20 in the muon momentum range 0.35 – 0.50 GeV/c.

In studying the lateral distribution of positive and negative muons, (Rebel, *et al.*, 2007), the lateral density was found to vary with, among other factors, the azimuth angle relative to the plane of the incident shower. The performed simulations used only proton and iron as the primary particles,

while the zenith angle was limited to 45° and the azimuth direction of arrival fixed at the four cardinal points: North, South East and West. In reality, however, the primary particles are incident from all ranges of zenith and azimuth angles. This leaves room for the studies of the rest of the values of azimuth angles as well as different ranges of zenith angles. This study therefore investigated the variation of the muon charge ratio with azimuth angle, at selected ranges of zenith angles.

Using the "MINOS near" detector, muons of both positive and negative charges were detected accurately in the MINOS experiment (de Jong, 2009). The charge ratio obtained from the flux of the detected muons varied considerably with the azimuthal angle. However, due to the East – West asymmetry of the detector, not much of the flux from the East or West could be detected. This made the observation of the East – West effect difficult.

The "MINOS near" experiment consists of a steel scintillating calorimeter detector located at 88° 16′ 14″ west longitude and 41° 51′ 26″ north latitude on the Fermilab campus. It is located 94.3 m underground and can accurately determine the charge sign of atmospheric muons, from which the muon charge ratio is determined. The experiment reported a mean muon charge ratio of $1.2666 \pm 0.0015(stat)^{+0.0096}_{-0.0088}(syst.)$ at a mean muon energy of 63 GeV.

2.2 Combinations of High and Low Energy models

In an investigation of hadronic interaction models with the KASCADE experiment aimed at investigating the reliability of air shower simulations, proton and iron were taken as assumptions for the primary particles (Milke *et al.*, 2006). The correlations of different components of air showers measured with the KASCADE experiment were investigated using several combinations of low-energy and high-energy interaction models in CORSIKA. It was found that the difference between the high-energy

models ($E_{lab} \geq 100$ GeV) had become smaller over the previous years, while there was only a small difference between the muon numbers generated by the low-energy models. However, there were still significant discrepancies between the high-energy hadronic interaction models DPMJET 2.55 and SIBYLL 2.1 on the one hand and QGSJET 01 on the other. SIBYLL and DPMJET predicted 6% fewer muons and 10 – 15% more electrons and hadrons than QGSJET (Kalmykov *et al.,* 1997). This suggests that updated versions of simulation models tend to reduce deviations from experimental results, although not eliminate them entirely. The results of this study are meant to investigate whether there is currently any further reduction in the discrepancy between the models.

Using version 5.20 of CORSIKA with the GHEISHA and VENUS (Werner, 1993) models as generators in the energy range 3 GeV to 20 GeV, it was found that the CORSIKA predictions on the charge ratio of muons showed a drop below 1 for very low muon momenta (Vulpescu *et al.*, 1999). This

was an obvious disagreement with the available experimental results, and needs further investigation. The muon charge ratio therefore proves to be a sensitive test variable in extensive air shower studies for the production model and propagation.

2.3 Effects of Different Primary Particles

In more recent studies (Hashim, 2007), simulation of EAS aimed at studying the response of the ALEPH apparatus to the measurement of cosmic ray muons was performed using CORSIKA and GALEPH. Muons with momenta not less than 10 GeV/c were considered. Their zenith angles were up to 20^{o} i.e. the muons were vertical . In comparing the measured data with theoretical expectations, the different hadronic interaction models gave different values of the muon charge ratio. SIBYLL (Fletcher *et al.*, 1994), which is known to generate relatively lower muon content, showed systematically higher values for the muon charge ratio. This is now known to be related to a too high multiplicity of K^{+} mesons in SIBYLL (Grupen *et*

al., 2008). On the other hand, the models VENUS and QGSJET described the data well; QGSJET was slightly low by about 10% (Grupen *et al.*, 2008). Since only protons were chosen as heavy particles in that work, there is therefore need for further investigation of the effects of heavier primary nuclei on the charge ratio of muons. In this study, zenith angles of up to 89° are used. This makes it possible to study the azimuthal effects on the charge ratio for both vertical and near horizontal muons.

In Monte Carlo simulations aimed at understanding the performance of the CosmoALEPH experimental set-up, Hashim (2007) investigated the variation of muon charge ratio with muon momentum for vertical muons (up to 50° zenith angle). The Monte Carlo simulations reproduced to a large extent the zenith and azimuthal angle distributions. Results for horizontal or near-horizontal muons are of interest since these muons undergo a greater degree of attenuation due to the longer paths they travel, compared to the vertical muons.

Apart from the latest study quoted (Grupen *et al.*, 2008), all the previous ones used versions of the simulation code CORSIKA, which have since been updated. This study has used a more recently updated version of CORSIKA. Hashim (2007) selected only protons as primary particles in the simulation code. This study has, in addition to the protons, selected helium and iron primaries.

3 METHODOLOGY

3.1 Theoretical Background

3.1.1 Production of Secondary Particles

High-energy primary cosmic ray nuclei interact with atmospheric nuclei to produce secondary particles:

$$A_{cr} + A_{air} \rightarrow \pi^{\pm}, \pi^{0}, K^{\pm}, \text{other hadrons} \quad (3.1)$$

where A_{cr} is a primary cosmic ray nucleus , A_{air} is an atmospheric nucleus, $\pi^{\pm}$ and π^{0} are charged and neutral pions respectively and $K^{\pm}$ are charged kaons (Kempa *et al.,* 2003). The secondary particles most abundantly produced are pions. Kaons are produced with a probability of 10 % compared to pions. Neutral pions initiate electromagnetic cascades in the soft component via their decay :

$$\pi^{0} \rightarrow \gamma + \gamma \quad (3.2)$$

where γ is a gamma ray photon. Charged pions and kaons can either initiate further interactions or decay to produce the muon and neutrino components :

$$\pi^+ \rightarrow \mu^+ + \nu_\mu \,, \quad \pi^- \rightarrow \mu^- + \bar{\nu}_\mu \quad \text{(mean lifetime } 2.6\times10^{-2}\,\mu s\text{)} \quad (3.3)$$

$$K^+ \rightarrow \mu^+ + \nu_\mu \,, \quad K^- \rightarrow \mu^- + \bar{\nu}_\mu \quad \text{(mean lifetime } 1.2\times10^{-2}\,\mu s\text{)} \quad (3.4)$$

where π^+ and π^- are positive and negative pions, K^+ and K^- are positive and negative kaons, μ^+ and μ^- are positive and negative muons and ν_μ and $\bar{\nu}_\mu$ are muon neutrino and muon antineutrino respectively. The muons are unstable hence they decay to produce electrons in the soft component, together with neutrinos.

$$\mu^+ \rightarrow e^+ + \nu_e + \bar{\nu}_\mu \qquad \text{(mean lifetime } 2.2\,\mu s\text{)} \qquad (3.5)$$

$$\mu^- \rightarrow e^- + \bar{\nu}_e + \nu_\mu \qquad \text{(mean lifetime } 2.2\,\mu s\text{)} \qquad (3.6)$$

where e^- and e^+ are electron and positron, ν_e and $\bar{\nu}_e$ are electron

neutrino and electron antineutrino respectively. Many other particles contained in cosmic rays are difficult to observe because their production cross sections are very low, and they are therefore produced at a low rate.

3.1.2 The East – West Effect

The primary cosmic radiation consisting of charged particles below 10 GeV energy shows directional effects caused by the Earth's magnetic field. This effect is also experienced by muons produced at high altitudes. Consider a particle of charge $z|e|$, velocity $\boldsymbol{v}$ and momentum $\boldsymbol{p} = m\boldsymbol{v}$ traveling in a circular equatorial path of radius r around a short dipole of moment M. The magnetic and centrifugal forces balance, hence:

$$z|e||\boldsymbol{B}\times\boldsymbol{v}|=\frac{mv^2}{r} \tag{3.7}$$

where $$B=\left(\frac{\mu_0}{4\pi}\right)\frac{M}{r^3} \tag{3.8}$$

If the velocity v is perpendicular to the magnetic field **B**, this gives a radius of orbit:

$$r_s = \left[\left(\frac{\mu_0}{4\pi} \right) \frac{Mz|e|}{p} \right]^{1/2} \tag{3.9}$$

The equation of motion of a particle as shown by Størmer is:

$$b = r \sin\theta \cos\lambda + \frac{\cos^2\lambda}{r} \tag{3.10}$$

where b is the closest distance, in Størmer units, that a tangent to the particle trajectory at infinity approaches the dipole axis, r is the distance of the particle from the dipole center in Størmer units, λ is the geomagnetic latitude and θ is the angle between the velocity vector **v** and its projection in the meridian plane co-moving with the particle. It is positive for particles traveling from East to West and negative for particles traveling in the

opposite direction. The condition b ≤ 2 determines which momenta are cut off by the Earth's field. Inserting b = 2 in equation (3.10), the equation for the cut-off momentum at any λ and θ is given by:

$$r = \frac{\cos^2 \lambda}{1+(1-\sin\theta \cos^3\lambda)^{1/2}} \tag{3.11}$$

The value of the particle momentum which makes the Earth's radius r_E equal to one Størmer unit is:

$$\frac{pc}{z} = \left(\frac{\mu_0}{4\pi}\right)\frac{Mc|e|}{r_E^2} \text{ GeV} \tag{3.12}$$

If all the quantities on the right hand side of equation 3.12 are expressed in S.I. units this leads to:

$$\frac{pc}{z} = 59.6 \text{ GeV} \tag{3.13}$$

At the magnetic equator, $\lambda=0$. For particles incident from the vertical, $\theta=0$ and $r=\frac{1}{2}\cos^2\lambda$. The vertical cut-off momentum $(\theta=0)$ is therefore given by :

$$(pc)=14.9\,z\cos^4\lambda \quad \text{GeV} \tag{3.14}$$

and therefore with the minimum value:

$$P_{min}=14.9 \quad \text{GeV/c} \tag{3.15}$$

The cut-off momentum for particles from the Eastern horizon $(\sin\theta=+1)$ is 59.6 GeV/c while that for particles from the western horizon $(\sin\theta=-1)$ is $59.6/\left(1+\sqrt{2}\right)^2=10.2$ GeV/c . Since the momentum cut – off for particles from the West is lower than that of

particles from the East, more positively charged particles arrive from the West than the East. This result is called the East-West effect. It is observed at all latitudes and at energies below 10 GeV (Perkins, 2005).

The East – West effect is transferred to muons, among other secondary particles of air showers induced in the atmosphere. The trajectories of positively charged muons traveling from East to West are bent up while for those traveling in the opposite direction are bent down, as a result of the influence of the geomagnetic field. The reverse is the case for negatively charged muons. The resulting different path lengths of the muons alter the decay probability and also the attenuation (Rebel, *et al.,* 2007).

3.1.3 Extensive Air Showers

Two or more coherent secondary particles (i.e. particles from the same origin hitting a detector) are sometimes observed, if their production is initiated by energetic primary particles. Such a phenomenon is called the

air shower. If the energy of a primary particle is at least 10^{14} eV, the total number of particles in a shower is very large, and the distance at which two or more particles are coherent may extend for as far as hundreds of meters. Such a shower is called the extensive air shower (EAS).

An extensive air shower has an electromagnetic, a muonic, a hadronic and a neutrino component. The shower nucleus consists of energetic hadrons, which inject energy into the electromagnetic and other components via interactions and decays. Neutral pions, which are produced in nuclear interactions and whose decay photons produce electrons and positrons via pair production, supply the electron, positron and photon component. Electromagnetic cascades are initiated when the process of bremsstrahlung produces photons. The photons cause pair production of positrons and electrons, and the two processes are repeated alternately. The decay of charged pions and kaons forms the muon and neutrino components (Hayakawa, 1969).

This sequence of multiplicative processes begins to decline as some of the particles receive energies that are too low to produce further particles effectively. Then the number of particles reaches a maximum and decreases with further increase in the thickness of matter traversed. The intensity of the particles increases sharply up to a maximum, after which it decays in a roughly exponential manner (Grupen, 2005).

3.1.4 The Muon Component of Extensive Air Showers

There are quite a number of muons reaching the ground which are very energetic. As they have long radiation lengths, they do not suffer many interactions in their travel paths from the points where they are created (~ 5 km altitude) to ground level. They have a much flatter lateral distribution than photons or electrons and they always dominate the signal at ground level for sufficiently large distances from the shower axis (Cazon *et al.*, 2004). This is particularly observed at lower primary energies, or in the

case of very inclined showers, where the electromagnetic component gets completely absorbed during the travel through the atmosphere, while the muons are able to survive the propagation through even larger slant depths. Thus the cosmic ray muons form a specific part of the natural background radiation, which affects material and biological substances . The radiation dose due to cosmic rays at ground level at average latitudes amounts to 0.35 milliSievert per year (Rebel *et al.*, 2007).

Since primary cosmic rays are positively charged, this excess positive charge is eventually transferred to muons. This results in a muon charge ratio greater than one. Assuming that primary protons interact with nuclei in the atmosphere to produce pions, the charge ratio of muons, $R=N(\mu^+)/N(\mu^-)$, can be theoretically estimated to be R = 1.25. However, experimental results over a wide momentum range, at sea level gives a constant value of $N(\mu^+)/N(\mu^-)\approx 1.27$.

3.2 Monte Carlo Simulations

3.2.1 Simulation Program

The simulation of extensive air showers is performed with the program CORSIKA (COsmic Ray SImulations for KAscade). CORSIKA is a program for detailed simulation of extensive air showers initiated by high-energy cosmic ray particles in the atmosphere. It was originally developed to perform simulations for the KASCADE experiment at Karlsruhe (Heck *et al*, 1998) and has been updated over the years. The primary particles used in this work are protons, helium and iron. The primary particles are tracked through the atmosphere until they undergo reactions with the air nuclei or – in the case of unstable secondaries – decay. The hadronic interactions at high energies in this work are described by the theoretical models VENUS, QGSJET, and SIBYLL. Those at lower energies are described by GHEISHA interaction routines. In particle decays, all branches down to the 1% level are taken into account. Electromagnetic interactions are not included.

3.2.2 Program Control and Run

At the beginning of the calculation, a set of parameters are chosen to control the simulation as specified in the steering card used in each simulation (see appendix 1). The primary particle is defined, and its energy selected at random in a particular energy range with the slope of the energy spectrum fixed at the value -2.7. Above an energy of a few GeV up to the 'knee' of the all-particle cosmic ray energy spectrum (see fig. 3.1) which is at approximately 10^{15} eV, the spectrum follows the power law (Perkins, 2005):

$$N(E)\,dE = const.\,E^{-\gamma}\,dE \tag{3.16}$$

where , γ is the cosmic rays spectral index, N is the number of cosmic rays at the "top" of the atmosphere and E is the cosmic ray particle energy. Hence the sampling is done such that in a given case, the primary sampled E_0 is given by (Rao and Sreekantan, 1998):

$$E_0=[E_1^{-\gamma}-R(E_1^{-\gamma}-E_2^{-\gamma})]^{-\frac{1}{\gamma}} \qquad (3.17)$$

where the sampling is done between the energy interval E_1 and E_2, and R is a random number initialized by the random number generator used in CORSIKA. The point of interaction t is given by $t=-\lambda \ln R$ g/cm^2 where λ is the mean free path and is measured in the units of g/cm^2. The all-particle cosmic ray energy spectrum is illustrated in figure 3.1.

The zenith and azimuth primary angles of incidence have been chosen at random from the fixed ranges of 0° – 89° and 0° – 360° respectively. A total of 10 observation levels have been defined and data on all particles penetrating these recorded as long as the energy exceeds a cut-off, specified for hadrons, muons, electrons or photons separately. Several flags select and control the hadronic interaction models at high energies and the respective cross sections; one flag selects the low energy hadronic interaction model.

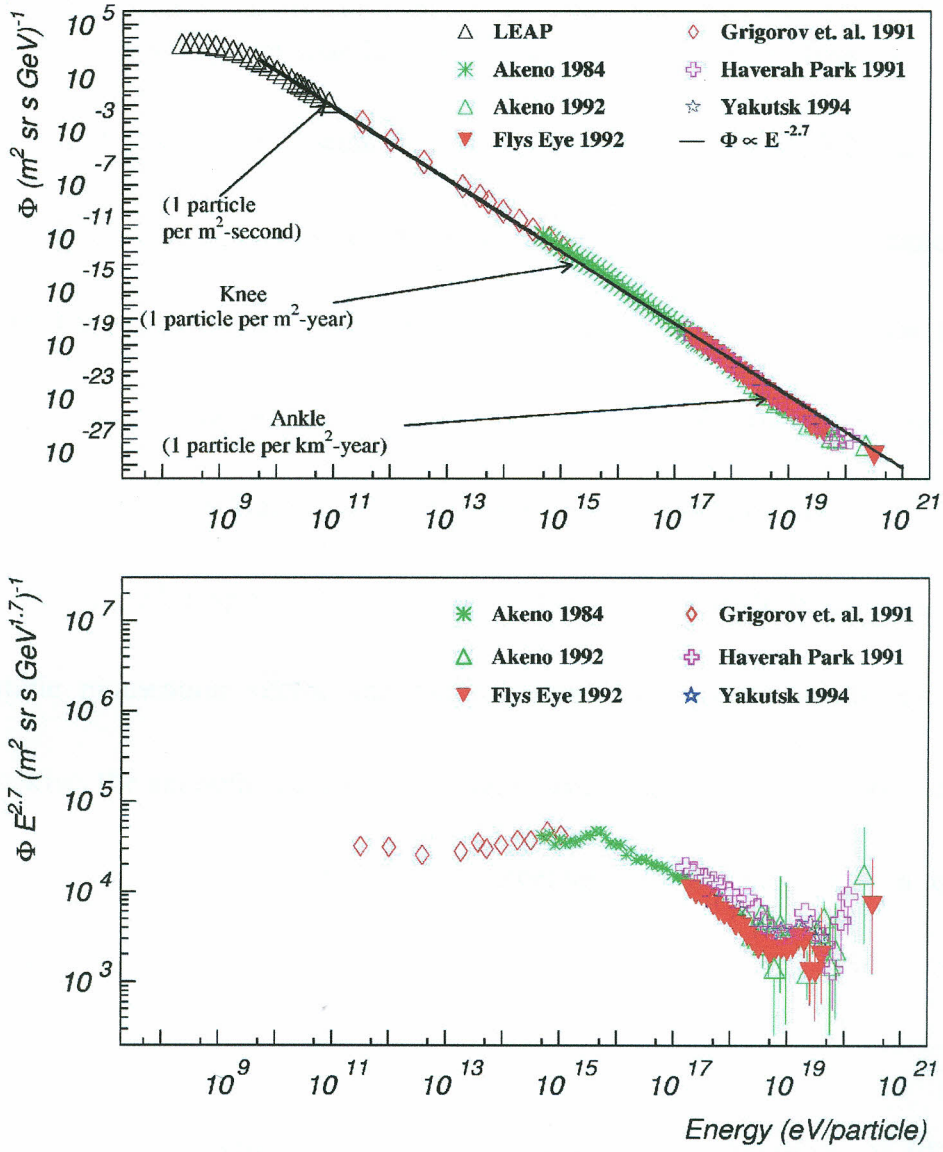

Fig. 3.1: The all-particle cosmic ray energy spectrum. (Source: Hashim (2007). Note the bending of the spectrum at E~10^{15} eV and E~10^{19} eV. These are known respectively as the 'knee' and 'ankle' on the spectrum.

3.2.3 Coordinate System

The coordinate system that has been used in this study is based on the CORSIKA coordinate system which is illustrated in figure 3.2. In the CORSIKA coordinate system, the x-axis is in the direction of the magnetic north, the y-axis points to the west and the z-axis upwards, while the sea level is taken as the origin. The Earth's magnetic field in this case is taken to be that of central Europe with horizontal and vertical components of 20.0 μT and 42.8 μT respectively. As figure 3.2 shows, the angle θ between the particle momentum vector and the negative z-axis is the zenith angle. Likewise, the azimuth angle ϕ is the angle formed by the positive x-axis and the x-y component of the particle momentum vector, measured in the anticlockwise direction.

This coordinate system has been modified to conform to that of the ALEPH experiment by turning the Cartesian plane through 90° in the anticlockwise direction , while maintaining the direction of the magnetic North.

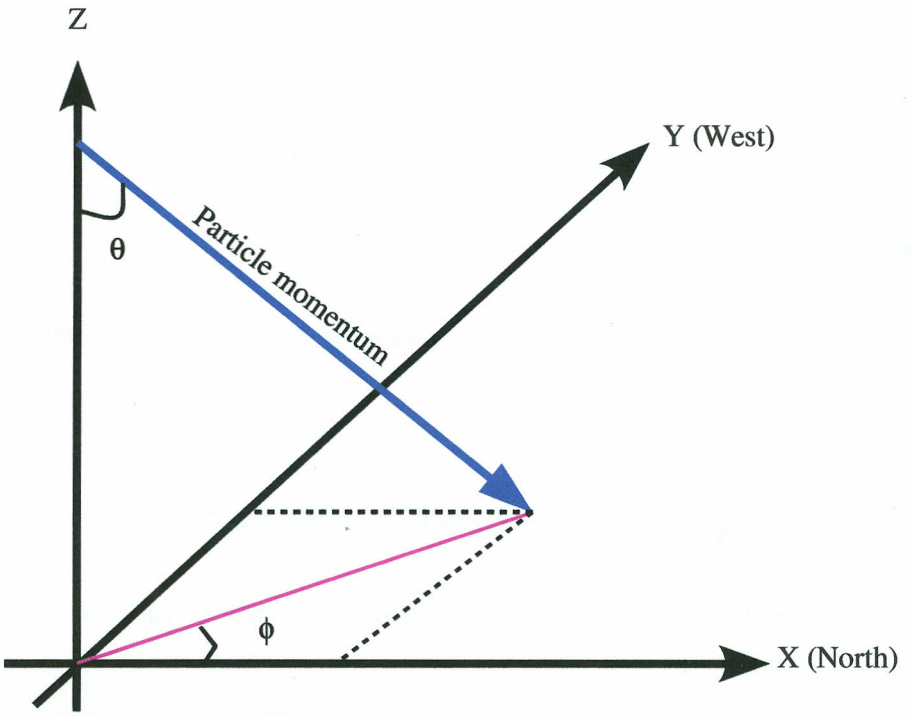

Fig. 3.2: An illustration of the coordinate system used in CORSIKA (Heck and Pierog, 2007). It has been modified in this study by turning the Cartesian plane through 90° in the anticlockwise direction such that all azimuth angles increase by 90°.

In this simulation, the Earth's atmosphere is modelled to be curved. This is necessary because zenith angles greater than 70° have been used. For angles greater than 70°, the use of a flat atmosphere would introduce significant errors although it would be simpler to perform shower calculations. In this atmosphere, the density variation with altitude is modelled by five layers. In the lower four layers, the density varies exponentially with the altitude. This gives a relationship between the mass overburden $T(h)$ of the atmosphere and the height h of the form:

$$T(h)=a_i+b_i e^{-h/ci} \qquad i=1,\ldots 4 \tag{3.18}$$

The parameters a, b and c of the U.S. atmosphere as obtained by J. Linsey are shown in table 3.1. In the fifth layer, there is a linear decrease of the mass overburden with height:

$$T(h)=a_5-b_5\frac{h}{c_5} \tag{3.19}$$

Layer i	Altitude h (km)	a_i (g/cm^2)	b_i (g/cm^2)	c_i (cm)
1	0... 4	-186.5562	1222.6562	994186.38
2	4 ...10	-94.919	1144.9069	878153.55
3	10 ...40	0.61289	1305.5948	636143.04
4	40 ...100	0.0	540.1778	772170.16
5	> 100	0.01128292	1	10^9

Table 3.1: Parameters of the U.S. standard atmosphere as obtained by Linsey (Heck *et al.*, 1998).

The U.S. standard atmosphere as parametrized by J. Linsey has been adopted in this work (Heck *et al.*, 1998).

3.2.4 Particle Tracking

The space and time coordinates of propagating particles between two interaction points, as well as their energy have been continually updated. Charged particles lose energy by ionization while neutral particles proceed without any energy loss. Due to the large penetration depth of positive and negative muons, a deflection resulting from multiple Coulomb scattering

has been taken into account. This is neglected for charged hadrons. The angular distribution of the multiple scattering is described by Moliere's theory, but may be approximated well by a Gaussian function.

The muon multiple scattering angle is selected by Moliere's theory where large steps are involved, but by adding many single Coulomb scattering events for small steps. In this approximation, and for a particular path, the mean square value of the polar scattering angle θ may be calculated using the expression:

$$\langle \theta^2 \rangle = \lambda \theta_s^2 \tag{3.20}$$

$$\text{with} \quad \theta_s^2 = \frac{1}{\lambda_s} \left(\frac{E_s}{m \gamma \beta^2} \right)^2 \tag{3.21}$$

where E_s = 0.021 GeV is the scattering constant, while m, γ and β are the mass, Lorentz factor and velocity in the laboratory respectively, λ

is the amount of matter traversed by the particle and λ_s = 37.7 g/cm^2. The velocity of light in this equation is set to unity, while the value of θ is picked at random according to the Gaussian distribution (Heck *et al.*, 1998):

$$P(\theta,\lambda)=\frac{1}{\sqrt{\pi\theta_s^2\lambda}}e^{-\theta^2/\left(\lambda\theta_s^2\right)} \tag{3.22}$$

All charged particle trajectories are bent in the Earth's magnetic field. If particles cross an observation level while being tracked to the next interaction point, their space, momentum and time coordinates are computed for the observation level and transferred to the particle output file. In the case of muons, the information at their point of production which is included in the output file includes: the type of muon i.e. whether positive or negative, the generation of the muon, the altitude of muon production, the momentum of the muon in the x-, y- and z-directions, its x-, y- and z-coordinates and the time since the first interaction. A minimum energy of

100 GeV is specified for a muon to be recorded as it passes an observation level.

A particle with charge Z and momentum $\vec{p}$ traveling along the path l in the magnetic field $\vec{B}$ suffers a deflection which points to the direction normal to the plane spanned by $\vec{B}$ and $\vec{p}$. The direction is changed by the angle α which, for small deflection angles, is approximately given by (Heck *et al.*, 1998):

$$\alpha \approx lZ \frac{\vec{p} \times \vec{B}}{p^2} \tag{3.23}$$

The angular deviation α is mainly caused by multiple Coulomb scattering. The process of multiple Coulomb scattering produces a deviation which increases with a decrease in momentum (Antonioli *et al.*, 1997).

3.2.5 Mean Free Path

The cross-section for a hadron interaction and the atmospheric density distribution along the flight path determine the distance a particle travels before it undergoes its next interaction or decay, called the mean free path. The mean free path for interactions is given by:

$$\lambda_{\text{int}} = m_{air} / \sigma_{n-air} \tag{3.24}$$

where $m_{air} = 14.54$ is the average atomic weight of air in g/mol, σ_{n-air} is the interaction cross section for the hadron-air interaction and λ_{int} is in g/cm^2. The probability that a muon will traverse a thickness λ of atmospheric layer without interaction is:

$$P_{\text{int}}(\lambda) = \frac{1}{\lambda_{\text{int}}} \exp(-\lambda / \lambda_{\text{int}}) \tag{3.25}$$

The corresponding probability for a muon to travel the distance l before it decays is:

$$P_D(l)=\frac{1}{l_D}\exp(-l/l_D) \tag{3.26}$$

where l has the dimensions of length. Path lengths of nucleons have been chosen at random from this probability distribution – for high energy nucleon-air interactions. At low energies, the interaction cross-sections have been interpolated from tables supplied with GHEISHA. Reduced energy resulting from slowing down of hadronic projectiles along their paths leads to a modified cross-section and free path. At higher energies, different parameterizations have been used in the hadronic interaction model employed. However, regardless of the model used, the cross-section has been taken as the weighted sum over the cross-sections σ_{n-N_i} of the three components of air namely N_2, O_2 and Ar with the percentage composition by volume of 78.1, 21.0 and 0.9 respectively . In this case:

$$\sigma_{n-air} = \sum_{i=1}^{3} n_i \sigma_{n-N_i} \qquad (3.27)$$

Since the analytic NKG formulas do not take into account the curvature of the Earth's surface in the treatment of the electromagnetic component, they have not been used in this work. Likewise, the EGS4 routines have not been applied. An enlarged multiple scattering step length factor has been used, for purposes of reducing the computing time.

4 RESULTS AND DISCUSSION

Calculations of muon flux, and hence the charge ratio of cosmic ray muons are presented in this chapter. The muon charge ratio is obtained as a result of extensive three – dimensional Monte Carlo simulations using version 6.6 of the program CORSIKA. A comparison is made with experimental data from the MINOS near detector and the WILLI detector.

The hadronic interaction models QGSJET II, SIBYLL and VENUS, which are available in CORSIKA, have been used to perform the simulations. For particle interactions below E_{lab}=80 GeV, the GHEISHA option is used. The range of zenith and azimuth angles are chosen as 0° - 89° and 0° - 360° respectively. Figure 4.1 shows the variation of the primary particles used and the muons produced with the zenith angle. It is observed that the variation of the number of muons produced with the zenith angle is not symmetrical as is the case with primary cosmic rays. This comes about due to the greater number of muons that undergo decays and attenuation at

larger zenith angles. This in turn is explained by the increased distance that the muons have to travel when they are more inclined, which increases their probability of decaying or interacting with atmospheric nuclei. The SIBYLL interaction model is observed to register relatively higher counts for muons produced compared to the other two models. This is now known to be due to its overestimation of the production cross section of muons.

The observation level used is 110 m, while an energy range of 100 GeV to 10^5 GeV is chosen. The observation level used is equal to the height above sea level at which the KASCADE experiment was conducted. This was aimed at providing a means of comparing the simulated data with experimental data. However, it turned out that the available statistics from the experimental data within the simulated energy range, and the range of zenith and azimuth angles, was very low. Since the energy chosen does not exceed the "knee" of the all-particle cosmic energy spectrum , the spectrum follows the power law given by equation 3.15.

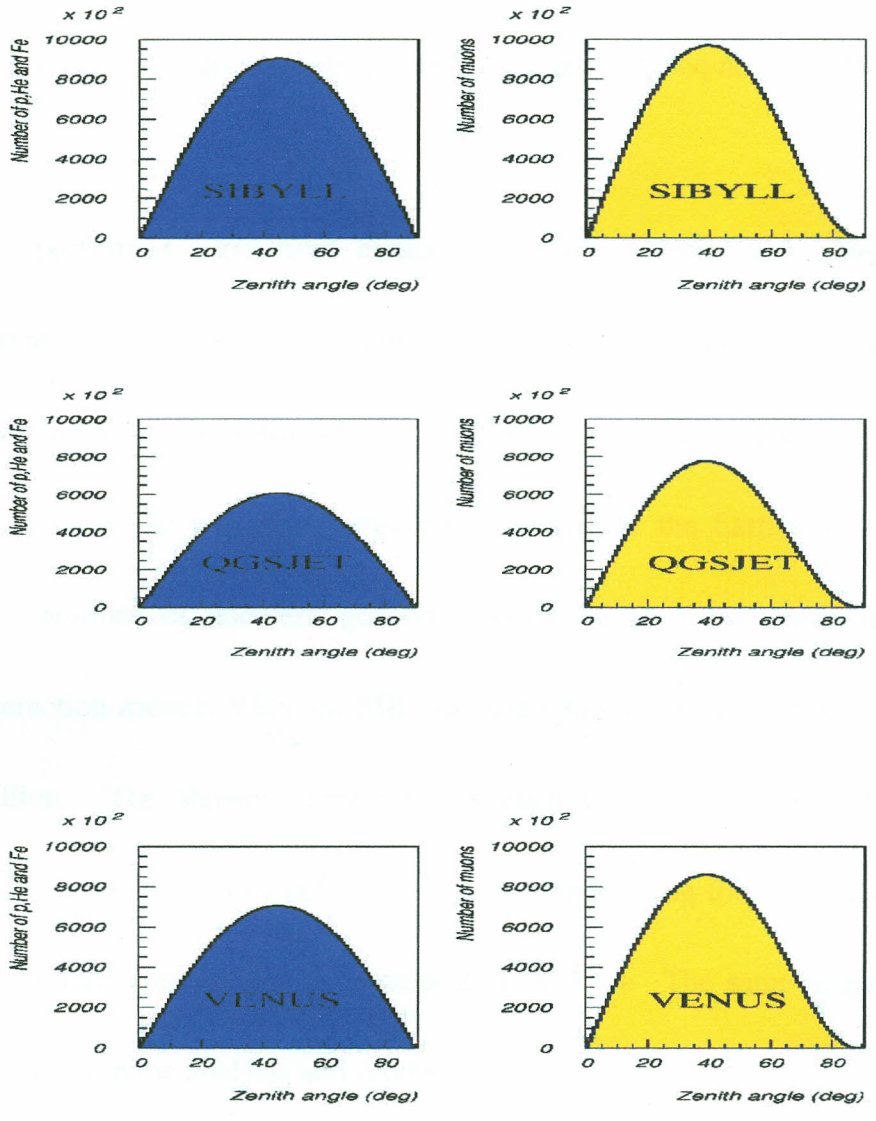

Fig. 4.1: variation of the zenith angle with the primary particles (protons, helium and iron) and secondary particles (muons) using the SIBYLL, QGSJET II and VENUS models. The primary particles are in the approximate ratio p:He:Fe = 85:12:3 which corresponds to the approximate ratio in the all-particle cosmic ray spectrum.

Hence an energy slope of -2.7 is used and the sampling is done such that in a given case, the primary energy sampled is given by equation 3.16.

The performed simulations comprise proton- , helium- and iron-induced extensive air showers, where the primary particles are taken in approximately the ratio 85:12:3. This corresponds to the ratio of the particles in the primary cosmic rays incident on the Earth's atmosphere. The number of showers generated using each of the three hadronic interaction models VENUS, SIBYLL and QGSJET II is approximately 50 million. The showers generated by each primary particle using each hadronic interaction model have been combined using the physics analysis workstation (paw) program version 2.14 of 2004. The same program has been used in the analysis and production of graphs.

In figure 4.2 are histograms which show the variation of the azimuth angle with the number of primary particles, and also muons as produced by the

three hadronic interaction models used. In these pairs of graphs, primary particles and muons from all zenith angles are included. The energy of the primary particles are from the entire range of energies considered in this study i.e. 100 GeV to 100 TeV.

It is observed that the distribution of both the primary and secondary cosmic ray particles is uniform across the entire range of azimuth angles. In this case, the East – West effect is obscured since many high-energy primary particles and muons are included in the statistics. The number of the very inclined (i.e. large zenith angle), low-energy muons therefore form only a small part of the total statistics.

The variation of energy with both the primary particles and the muons produced is shown in figure 4.3, where the slope of the graph of the primary particles is set in the steering card according to the all-particle cosmic ray spectrum to be -2.7.

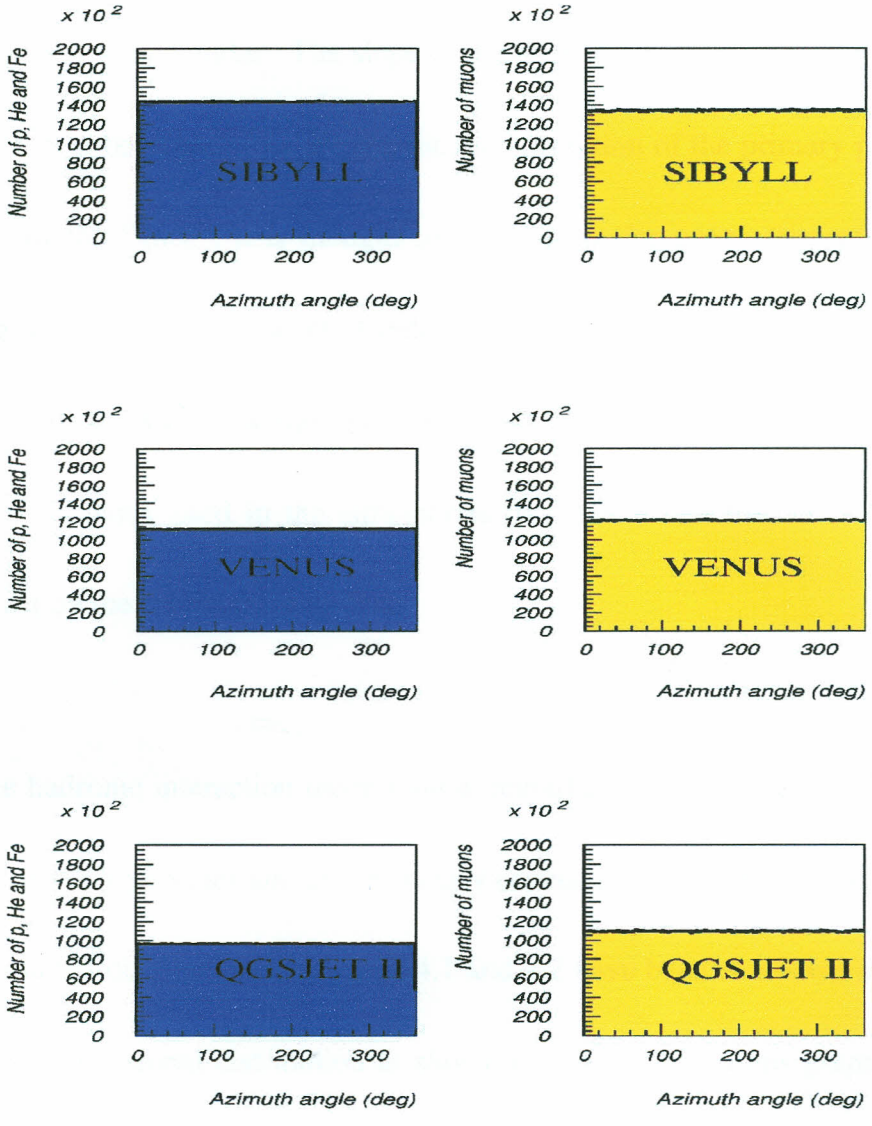

Fig. 4.2: Variation of the azimuth angle with the number of primary cosmic ray particles and muons using the SIBYLL, VENUS and QGSJET II interaction models.

The slope of the graph of the resulting secondary particles (muons) is observed to be similar. The slope of the all-particle cosmic ray spectrum is known to be sensitive to the chemical composition of the primary particles. Below the "knee", it is thought to be constant for every element. In this region, the combined spectral index for all primary cosmic ray particles is -2.7 but the value for individual elements differs. Hence the value of the spectral index used in the simulations for helium and iron does have an effect on the resultant muon flux.

The hadronic interaction models show remarkably similar features for both the primary particles and the secondary cosmic ray particles. The zenith and azimuthal distributions in figures 4.1 and 4.2 have been combined to give a three-dimensional distribution as shown in figure 4.5. In this graph, the z-axis is represented by the scale on the right of each graph.

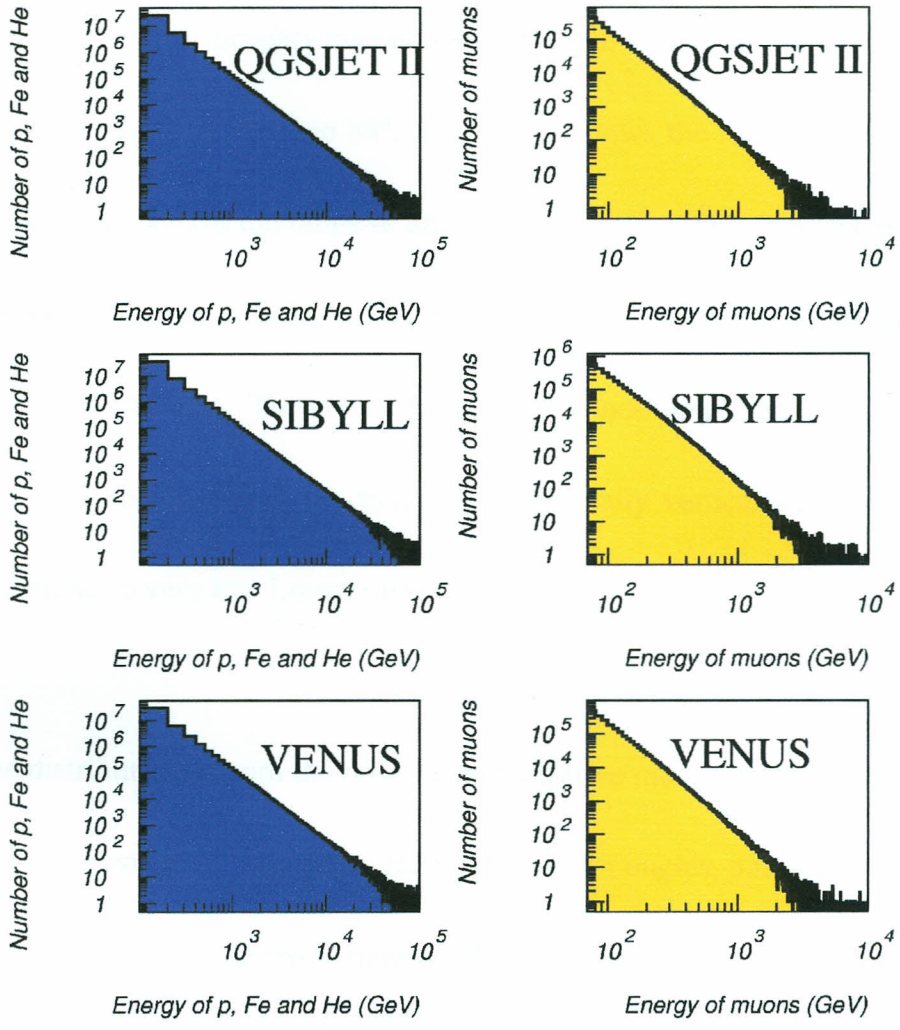

Fig. 4.3: Variation of the primary energy and the energy of the muons produced with the total number of primary particles (protons, helium and iron) using the hadronic interaction models QGSJET II, SIBYLL and VENUS. The slope of the primary spectrum is set at -2.7.

The number of positively and negatively charged muons has been reconstructed for primary cosmic rays falling in "slices" of zenith angles in intervals of 10° from 0° to 89°. Figure 4.4 shows the flux of positive and negative muons for the range of azimuth angles 0° – 360°, incident at zenith angles within the range 0° to 10°, produced using each of the three hadronic interaction models. The muons have energies not more than 100 GeV. At such low zenith angles, the muons are practically vertical and hence they experience a very low Lorentz force.

The distribution of both the positive and negative muons is therefore almost uniform throughout the whole range of azimuth angles, although there are more positive than negative muons. This is attributed to the fact that in the East – West plane, the trajectories of the positively charged muons arriving from the West are bent up while those of negatively charged muons are bent down due to the influence of the Earth's magnetic field. The opposite of this is the case for muons arriving from the East.

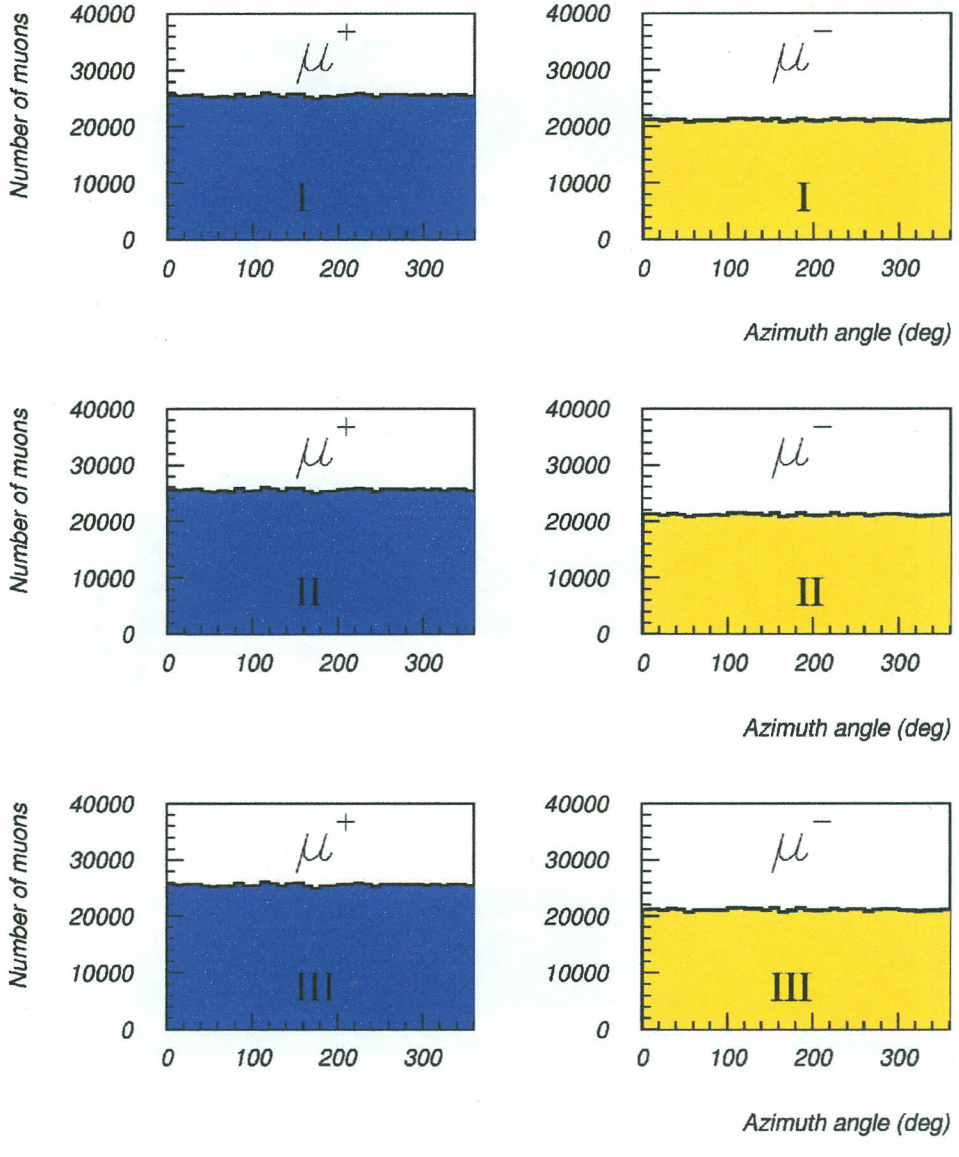

Fig.4.4: Azimuthal distribution of positively and negatively charged muons with energies up to 100 GeV incident at zenith angles 0° - 10° using (I) VENUS, (II) SIBYLL and (III) QGSJET II hadronic interaction models.

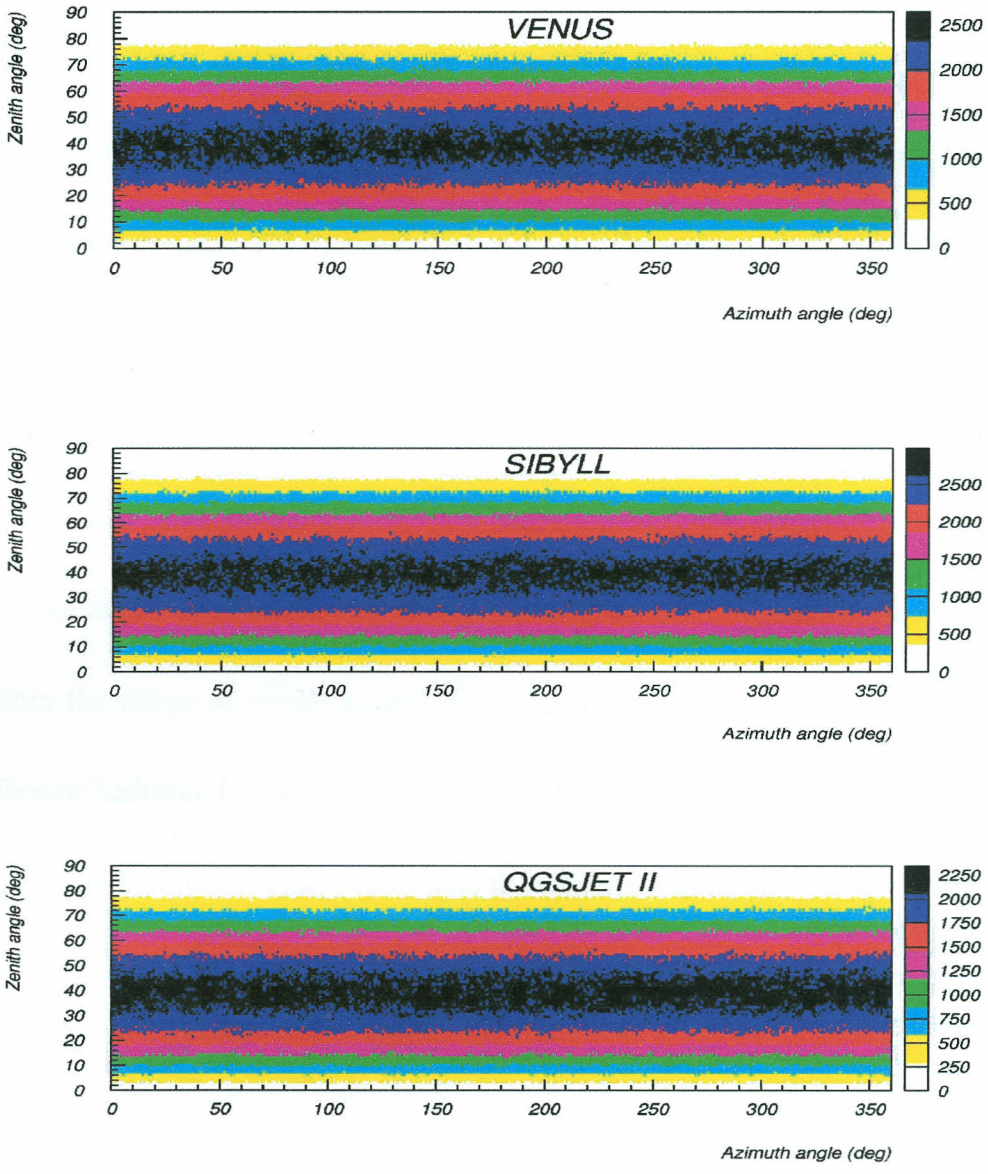

Fig. 4.5: Three dimensional variation of muons flux with zenith and azimuth angles for the hadronic interaction models VENUS, SIBYLL and QGSJET II.

The decay probability of positively charged muons is therefore modified differently from that of negatively charged muons, resulting in a larger number of positively than negatively charged muons reaching the observation level.

From the numbers of positively and negatively charged muons, the muon charge ratio has been calculated. The variation of muon charge ratio with azimuth angle for muons with energy up to 100 GeV, which are incident within the range of zenith angles 0^{o} - 10^{o}, is shown in figure 4.6 for the different hadronic interaction models. The SIBYLL model gives a notably higher value of muon charge ratio than the other two models.

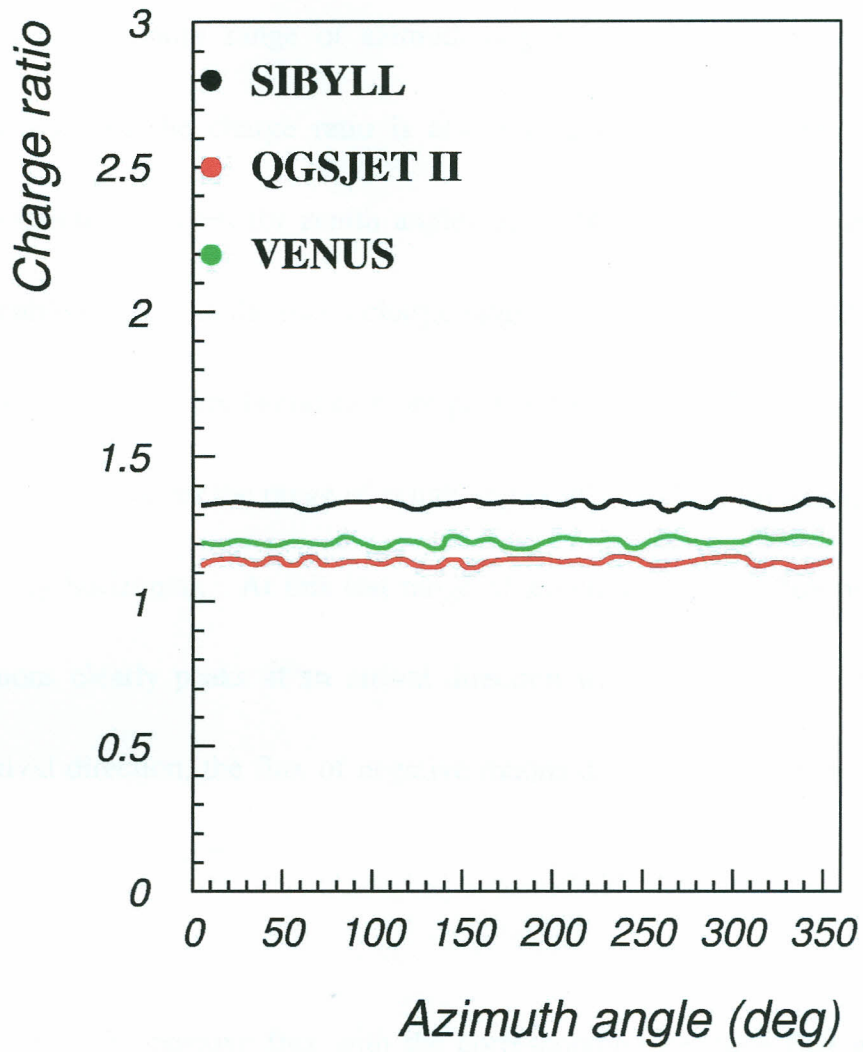

Fig. 4.6: Azimuthal dependence of charge ratio for muons with energies up to 100 GeV which are incident at zenith angles within the range 0° - 10° using the SIBYLL, QGSJET II and VENUS interaction models.

Given the relatively uniform distribution of positive and negative muons across the entire range of azimuth angles as shown in figure 4.4, the variation of the charge ratio is also predictably similar. This trend of variation is evident for zenith angles up to 60°. Between 60° and 70°, a notable increase in the muon charge ratio is observed at about 180° azimuth angle. This pattern becomes more pronounced for zenith angles 70° - 80°, and very clear for the range of zenith angles 80° - 89° i.e. for muons that are nearly horizontal. At this last range of zenith angles, the flux of positive muons clearly peaks at an arrival direction which is West. At the same arrival direction, the flux of negative muons drops to a minimum. This is shown in figure 4.7.

Dividing the positive flux with the corresponding negative flux gives the azimuthal variation of the simulated muon charge ratio. Figure 4.8 shows a comparison of the results obtained for very inclined muons (zenith angles between 80° and 90°) using the hadronic interaction models QGSJET II,

SIBYLL and VENUS, where a pronounced East – West effect is evident. It is observed that at zenith angles up to 60°, the East – West effect is not noticeable, but at zenith angles greater than this, the phenomenon of East – West effect becomes more and more evident using all the three models, as shown in figures 4.9 – 4.11. The phenomenon becomes very clear in the last range of zenith angles as seen in all the three sets of graphs.

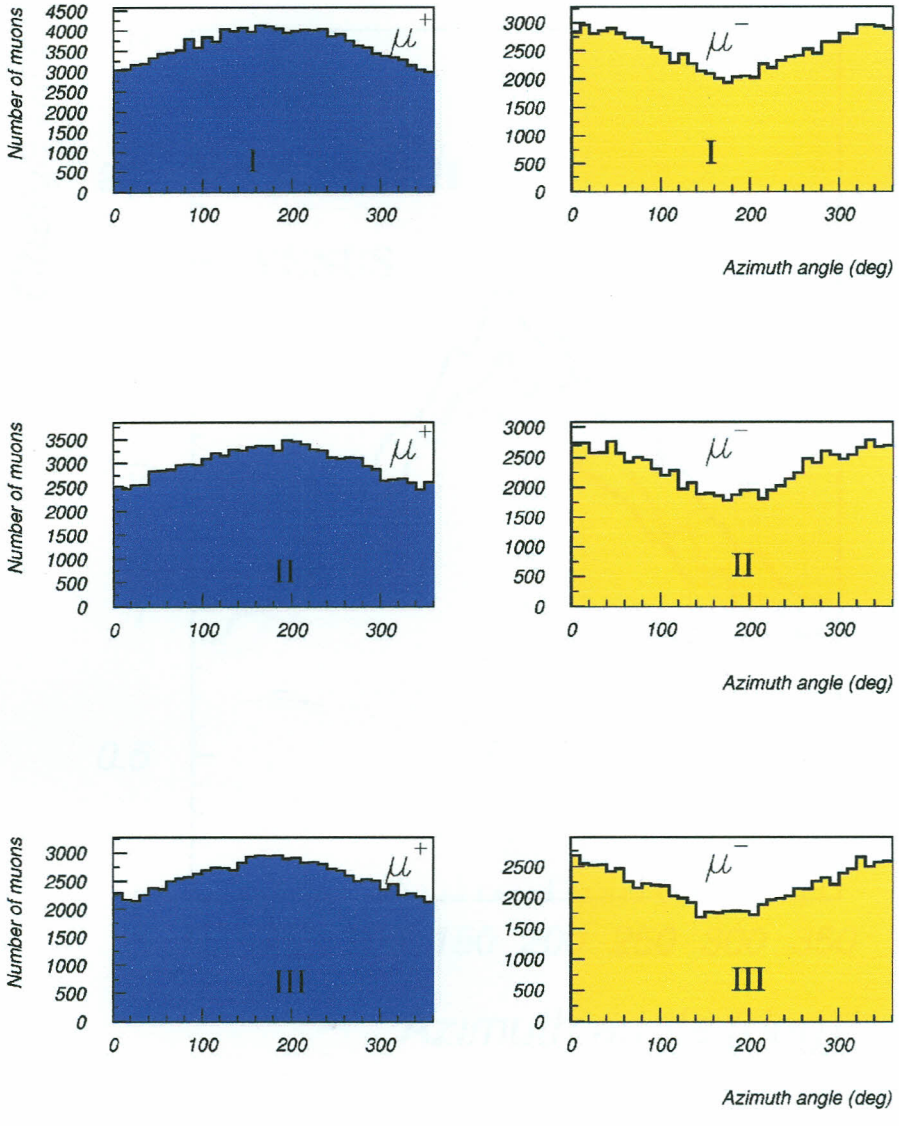

Fig. 4.7: Flux of positive and negative muons with energy up to 100 GeV arriving at zenith angles 80° - 89° using the hadronic interaction models (I) SIBYLL, (II) VENUS and (III) QGSJET II respectively.

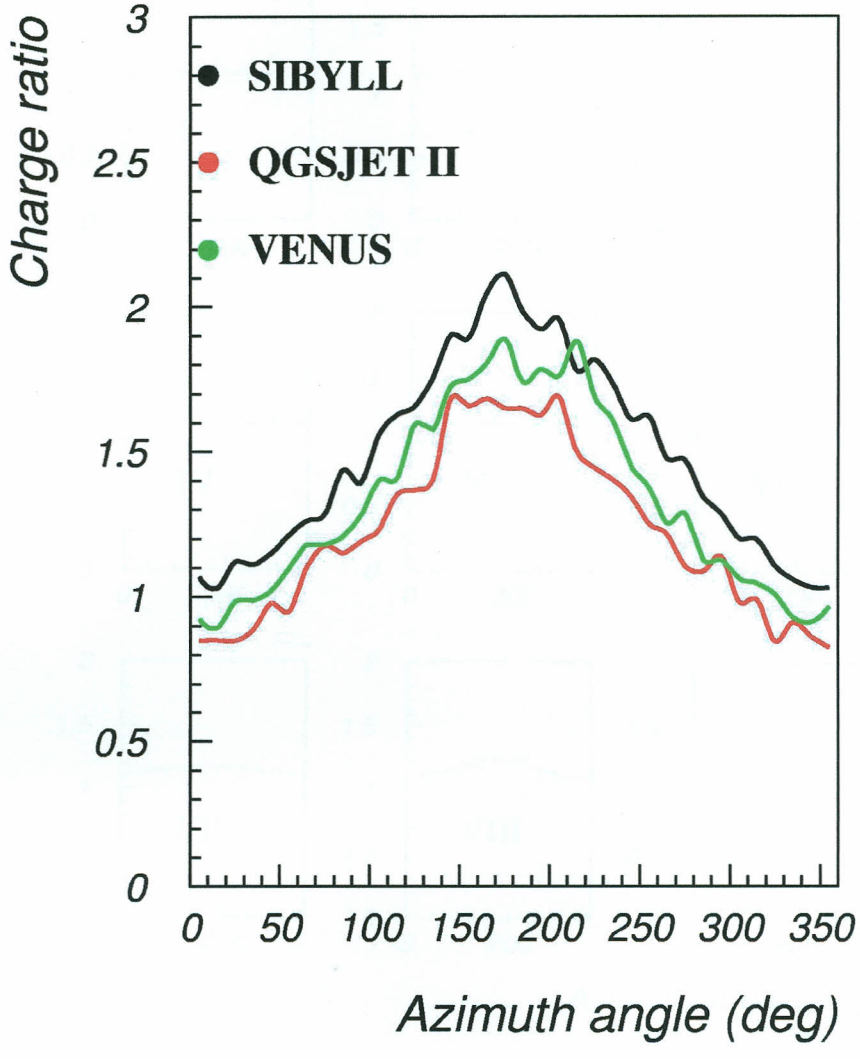

Fig. 4.8: A comparison of the charge ratio as simulated by the hadronic interaction models SIBYLL, QGSJET II and VENUS for the range of zenith angles 80°–89° The primary particles used are p, He and Fe in the ratio 85:12:3 based on the composition of the primary energy spectrum.

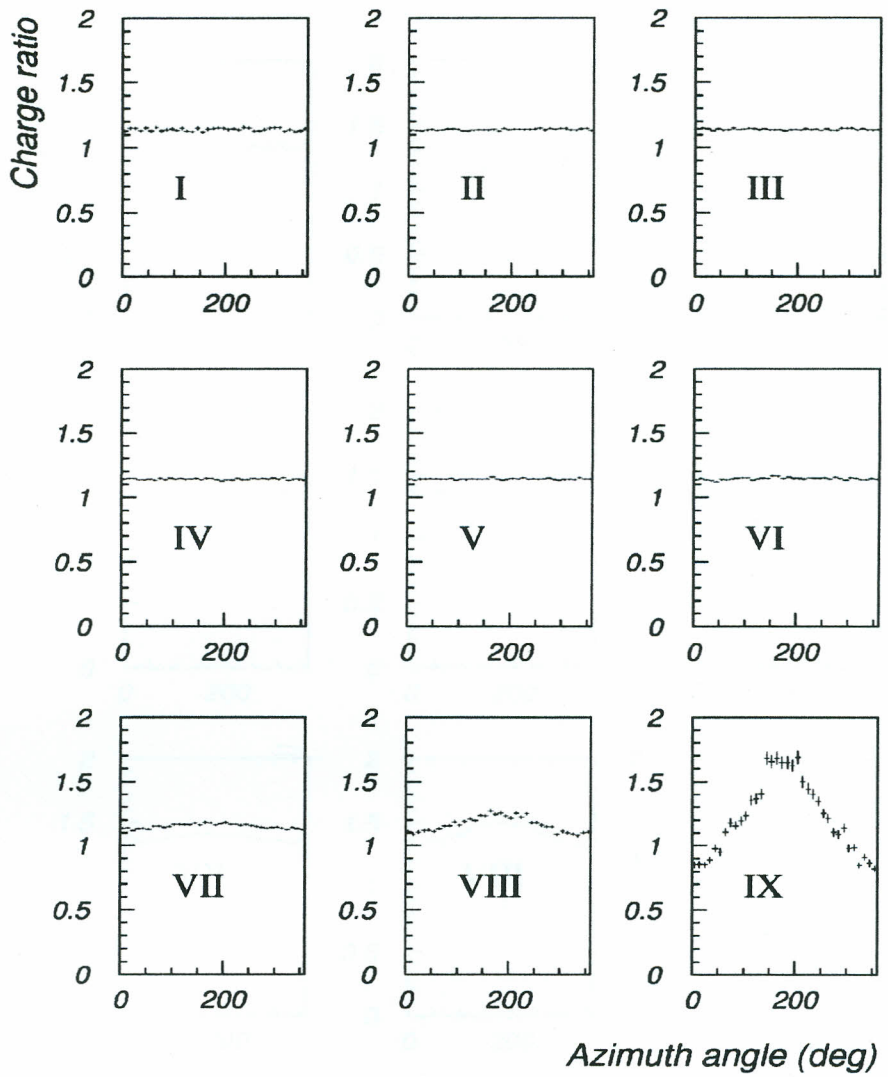

Fig. 4.9: Charge ratio simulated at zenith angles (I) $0^0<\theta\leqslant10^0$, (II) $10^0<\theta\leqslant20^0$, (III) $20^0<\theta\leqslant30^0$,(IV) $30^0<\theta\leqslant40^0$, (V) $40^0<\theta\leqslant50^0$, (VI) $50^0<\theta\leqslant60^0$, (VII) $60^0<\theta\leqslant70^0$, (VIII) $70^0<\theta\leqslant80^0$, (IX) $80^0<\theta\leqslant90^0$ using the QGSJET II model (the data is in appendix II Fig. A2.1 – A2.3).

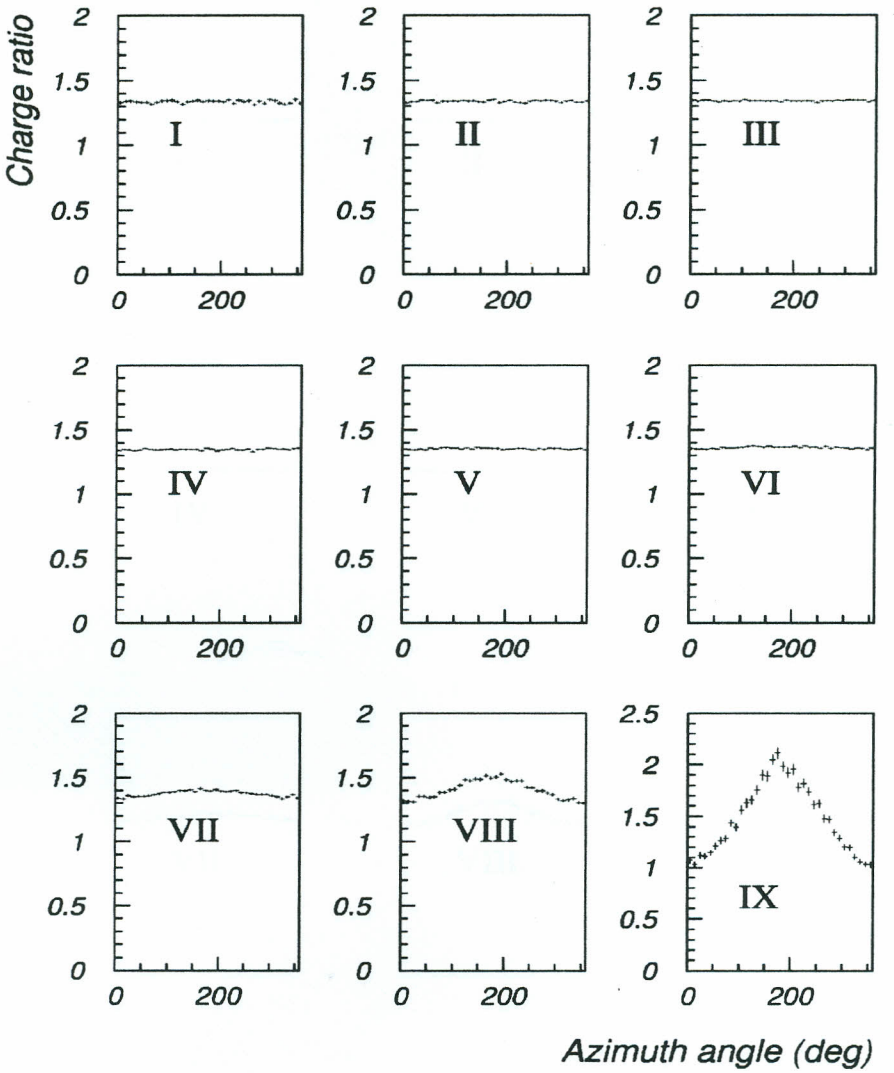

Fig. 4.10: Charge ratio simulated at zenith angles (I) $0^0<\theta\leqslant10^0$, (II) $10^0<\theta\leqslant20^0$, (III) $20^0<\theta\leqslant30^0$,(IV) $30^0<\theta\leqslant40^0$, (V) $40^0<\theta\leqslant50^0$, (VI) $50^0<\theta\leqslant60^0$, (VII) $60^0<\theta\leqslant70^0$, (VIII) $70^0<\theta\leqslant80^0$, (IX) $80^0<\theta\leqslant90^0$ using the SIBYLL model (the data is in appendix II Fig. A2.4 – A2.6).

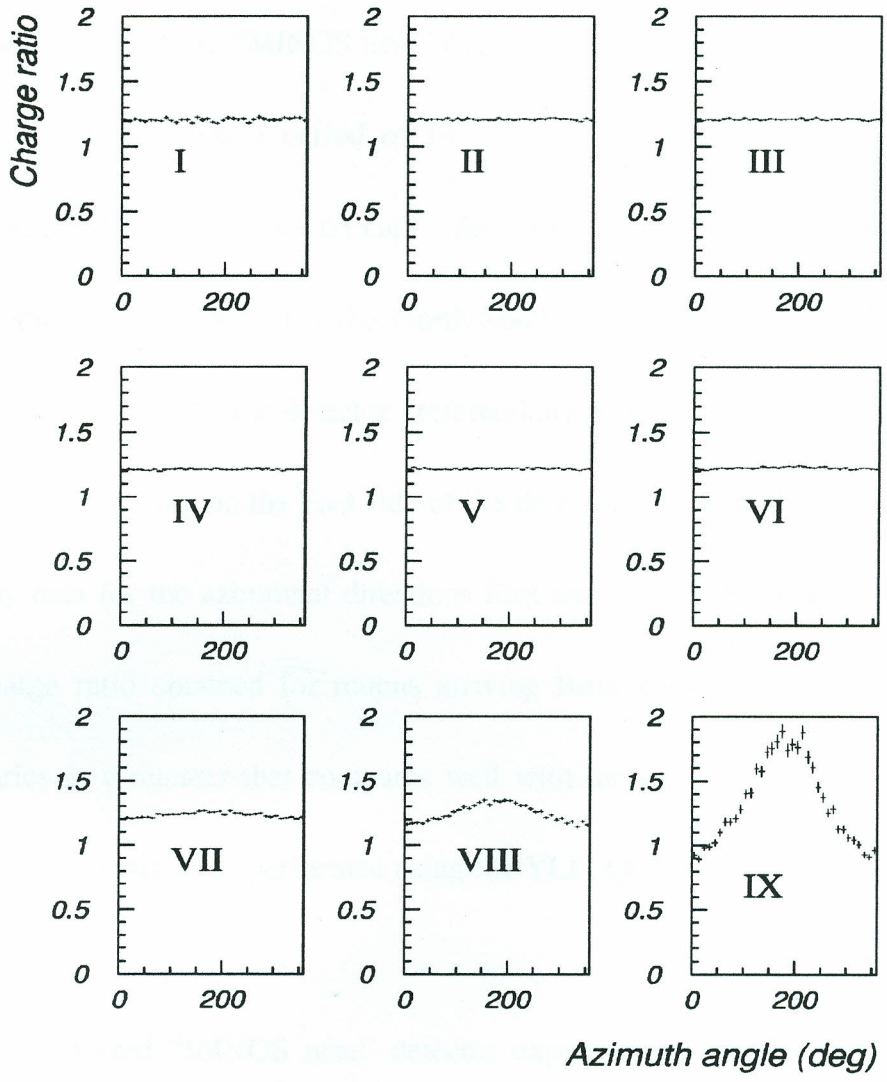

Fig. 4.11: Charge ratio simulated at zenith angles (I) $0^0<\theta\leqslant10^0$, (II) $10^0<\theta\leqslant20^0$, (III) $20^0<\theta\leqslant30^0$,(IV) $30^0<\theta\leqslant40^0$, (V) $40^0<\theta\leqslant50^0$, (VI) $50^0<\theta\leqslant60^0$, (VII) $60^0<\theta\leqslant70^0$, (VIII) $70^0<\theta\leqslant80^0$, (IX) $80^0<\theta\leqslant90^0$ using the VENUS model (the data is in appendix II Fig. A2.7 – A2.9).

The figure 4.12 shows the variation of charge ratio with azimuthal angle, as obtained using the "MINOS near" detector. The graph was obtained using data collected over a period of 190.2 days between 2006 and 2008, for muons of average energy 63 GeV. As a result of the East-West asymmetry of the detector, and also the North-South asymmetry introduced by the spectrometer used, the detector preferentially reconstructed northerly going muons occurring on the East side of the detector. There is therefore hardly any data for the azimuthal directions East and West. However, the muon charge ratio obtained for muons arriving from the other azimuth angles varies in a manner that compares well with the predictions of the Monte Carlo simulations as performed using SIBYLL, QGSJET and VENUS.

The analyzed "MINOS near" detector experimental data is compared to predictions of QGSJET II, SIBYLL, and VENUS models based on about 50 million simulated events for each model.

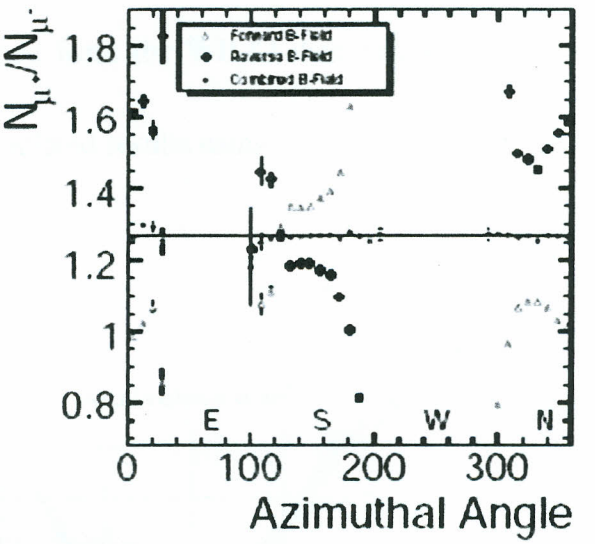

Fig 4.12: Charge ratio as a function of azimuth angle as obtained using the "MINOS near" detector (de Jong, 2009). The East of this detector coordinate system is equivalent to West in the CORSIKA coordinates, while its West is equivalent to East in CORSIKA. Note the similarity between the charge ratio for the combined field and that in fig. 4.6. Note also the gap in charge ratio for the East and West directions due to scarcity of data.

A low statistical accuracy for muons arriving from the East and West leads to two gaps in the graph of variation of charge ratio with azimuth angle. However, for the rest of azimuth angles, the slight fluctuations in the charge ratio compare quite well with the simulated results obtained using all the

three hadronic interaction models used in this study, as shown in figure 4.6. The data obtained from the WILLI detector, which is inclined at 45° , is compared to simulated results using CORSIKA in figure 4.13.

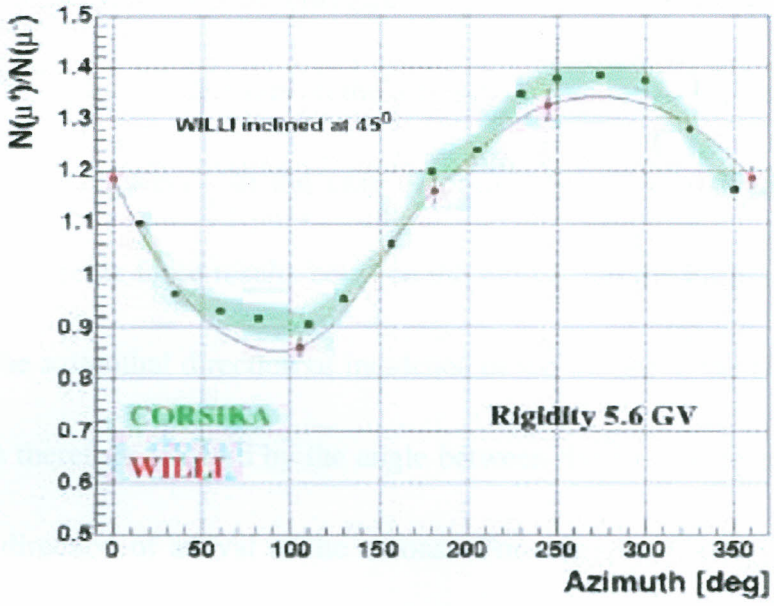

Fig. 4.13: Azimuth dependence of muon charge ratio from the WILLI detector compared to CORSIKA simulations (Mitrica *et al.* 2006). The muons from the WILLI detector are incident from the four azimuthal directions: North, East, South and West. The zenith angle is fixed at 45°.

The pronounced East – West effect observed by WILLI is well reproduced by the CORSIKA simulations, based on the DPMJET hadronic model.

5 CONCLUSIONS AND RECOMMENDATIONS

5.1 Conclusions

The azimuthal variation of the muon charge ratio in extensive air showers is strongly influenced at muon energies of up to 100 GeV by the geomagnetic field. This influence depends on the azimuthal direction of incidence of the extensive air showers. In the case of positively and negatively charged muons, a Lorentz force results between the muons and the Earth's magnetic field. The azimuthal direction of incidence of the muons at the observation level are therefore affected by the angle between the Earth's magnetic field and the direction of arrival of the muons. For example, the Lorentz force acting on positively charged muons from the North is directed towards the East, while those from the south are deflected in the opposite direction. Due to the inclination of the Earth's magnetic field, this effect is mainly observed in muons that are incident on the observation plane at large zenith angles i.e. nearly horizontal. In the case of smaller zenith angles, i.e. less than 80°, there is only a slight variation in the muon charge ratio with the

azimuth angle. This indicates that the Earth's magnetic field has a negligible influence on the nearly vertical positively and negatively charged muons.

The detailed knowledge of the cosmic ray muon charge ratio for muons produced by primary cosmic rays of energy 100 GeV to 100 TeV is still limited by the experimental statistics available. Therefore a reasonable agreement between the simulated charge ratio and values obtained from data as found in this study may be considered as a validation of the CORSIKA treatment of the magnetic field effects. In particular, the East – West effect of the muon component of extensive air showers is confirmed for low energy, inclined muons.

5.2 Recommendations

Considering the comparison between the simulated and experimental results of the East – West effect on the cosmic ray muons in extensive air showers,

the following recommendations are made:

(i) Further experimental investigation of the East – West effect on low-energy inclined muons should be carried out so as to obtain a more reasonable amount of experimental data.

(ii) A further comparison should be made between the experimental data obtained and the simulated results for purposes of validating the hadronic interaction models.

(iii) An investigation of the effect of using the same spectral index γ on different elements and how it affects the muon charge ratio.

REFERENCES

Antonioli, P., Ghetti, C., Korolkova, E. V., Kudryavtsev, G., Sartorelli, G. (1997). A three dimensional code for muon propagation through rock: MUSIC. *Astroparticle Physics* 7:357 – 368.

Bahmanabadi, M., Ghomi, M. Khakian and Sheidaei, F. (2005). Experimental studies of positive and negative atmospheric muons with a cosmic rays telescope. *Astroparticle Physics* 24:183 – 190.

Berezinskii, V.S., Bulanov, S.V., Dogiel, V.A., Ginzburg, V.L.and Ptuskin, V.S. (1990) *Astrophysics of cosmic rays.* Amsterdam: North Holland Elsevier Science Publishers B.V. Pp 1 – 3.

Brancus, I.M., Wentz, J., Mitrica, B., Rebel, H., Petcu, M., Bozdog, H., Mathes, H.J., Badea, A.F., Bercuci, A., Aiftimiei, C., Duma, M., Meli, A., Toma, G. and Vulpescu, B. (2003). The East-West effect of the muon charge ratio at energies relevant to the atmospheric neutrino anomaly. *Nuclear Physics* A721: 1044c-1047c.

Cazon, L., Vazquez, R.A. and Zas,E. (2005). Depth development of extensive air showers from muon time distributions. *Astroparticle Physics* 23: 393 – 409.

Cazon, L., Vazquez, R.A., Watson, A.A.and Zas, E. (2004). Time structure of muonic showers. *Astroparticle Physics* 21:71-86.

de Jong, J.K. (2009). The atmospheric muon charge ratio at the MINOS Near detector. *Proceedings of the 31st ICRC, LODZ 2009.*

Engel, R. (2002) *Computer Physics Communications* 147:465-470.

Fesefeldt, H. Report **PITHA-85/02** (1985), RWTH *Aachen*

Fletcher, R.S., Gaisser, T.K., Lipari, P.and Stanev, T. (1994). *Phys. Rev.* **D50** 5710;

Grupen, C. (2005) *Astroparticle Physics.* Berlin: Springer-Verlag. Pp 142-150.

Grupen,C., Hashim, N.O., Jost, B., Maciuc, S., Luitz, A., Mailov, A., Muller, A.S., Putzer, A., Rensch, B., Sander, H.G., Schmeling, S., Schmeling, M., Tcaciuc, R., Wachsmuth, H., Ziegler, Th. and Zuber, K. (2008). Cosmic ray results from the CosmoALEPH experiment. *Nuclear Physics B (Proc. Suppl.)* 175-176, 286-293.

Hashim, N.O. (2007). Measurement of the Momentum Spectrum of Cosmic Ray Muons at a depth of 320 mwe. *PhD Thesis Universität Siegen.* .

Hayakawa, S. (1969). *Cosmic Ray Physics.* New York: John Wiley & Sons. Pp 441-450.

Heck, D., Knapp, J., Capdevielle, J.N., Schatz, G. and Thouw, T. Wissenschaftliche Berichte FZKA 6019. (1998). CORSIKA: A Monte Carlo Code to Simulate Extensive Air Showers. Karlsruhe: Pp 5-6, 59 .

Heck, D and Pierog, T. (2007). Extensive Air Shower Simulation with CORSIKA: A user's guide. Karlsruhe: Forschungszentrum Karlsruhe GmbH. Pp 84.

Kalmykov, N.N., Ostapchenko, S.S. and Pavlov, A.I. (1997). *Nucl. Phys. B (Proc. Suppl.)* **52B:** 17

Kempa, J. and Brancus, I.M. (2003). Zenith angle distributions of cosmic ray muons. *Nuclear Physics B (Proc. Suppl.)* 122: 279-281.

Milke, J., Antoni, T., Apel, W.D., Badea, F., Bekk, K., Bercuci, A., Bluemer, H., Buzdog, H., Brancus, I.M., Büttner, C., Chilingarian, A., Daumiller, K., Doll, P., Engel, R., Engler, J., Feβler, F., Gils, H.J., Glasstetter, R., Haungs, A., Heck, D., Hörandel, J.R., Kampert, K.H., Klages, H.O., Maier, G., Mathes, H.J., Mayer, H.J., Müller, M., Obenland, R., Ochlschläger, J., Ostapchenko, S., Petcu, M., Rebel, H., Risse, A., Risse, M., Roth, M., Schatz, G., Schieler, H., Scholz, J., Thouw, T., Ulrich, H., Van Buren, J., Vardanyan, A., Weindl, A., Wochcle, J. and Zabierowski, J. (2006). Investigation of hadronic interaction models with the KASCADE experiment. *Nuclear Physics B (Proc. Suppl.)* 151: 469-472.

Mitrica, B., Brancus, I.M., Rebel, H., Wentz, J., Bercuci, A., Toma, G., Aiftimiei, C. and Duma, M. (2006). Experimentally guided Monte Carlo calculations of the atmospheric muon and neutrino flux. *Nuclear Physics B (Proc. Suppl.)* 151: 295-298.

Perkins, Donald H. (2005) *Particle Astrophysics.* New York: Oxford University Press.

Ranft, J., (1995).*Phys. Rev* **D51:**64; preprint *hep-ph/9911213* and *hep-ph/9911232* (1999)

Rao, M.V.S. and Sreekantan, B.V. (1998) *Extensive Air Showers.* Singapore: World Scientific Publishing.

Rebel, H., Sima, O., Haungs, A., Oehlschlager, J., Manailescu, C., Morariu, C. and Patrascioiu, A. (2007). The muon charge ratio in cosmic ray air showers. *Forschungszentrum Karlsruhe FZKA 7294.*

Sommers, P. (2004). Extensive Air Showers and measurement techniques. *CR physique* 5 : 463 – 472.

Vulpescu, B., Wentz, J., Badea, A.F., Bozdog, H., Brancus, I, M., Duma, M., Haungs, A., Mathes, H.J., Petcu, M., Rebel, H., and Roth, M. (1999). The charge ratio of cosmic ray muons. *Nuclear Physics B (Proc. Suppl.)* 75 A: 324 – 326.

Werner, K. (1993). *Phys. Rep.* **232:** 87

APPENDIX I

SAMPLE STEERING CARD FOR EAS SIMULATIONS USING CORSIKA

```
NUMBER OF VERSION  : 6.598
 DATE  OF VERSION     : April    20, 2007

 VERSION GENERATED FOR UNIX OR COMPATIBLE SYSTEMS
 ^^^^^^^^^^^^^^^^^^^^^^^^^^^^^^^^^^^^^^^^^^^^^^^^^^^^^^^^
  (RECL IS DEFINED IN BYTES)
  WITH NEW DATE_AND_TIME ROUTINE
 ZENITH ANGLE DEPENDENCE FOR FLAT DETECTOR ARRAY

 CURVED VERSION WITH SLIDING PLANAR ATMOSPHERE
 ==============================================

 PARTICLE OUTPUT IS WRITTEN IN COMPACT FORM
 ==========================================


 ========== USERS RUN DIRECTIVES FOR THIS SIMULATION
============================


 DATA CARDS FOR RUN STEERING ARE EXPECTED FROM

STANDARD INPUT

RUNNR   300002                  run number
EVTNR   1                       number of first shower event
```

```
NSHOW  1000000                number of showers to generate
PRMPAR 14                     particle type of prim. particle
ESLOPE -2.7                   slope of primary energy spectrum
ERANGE 1.E2 1.E5              energy range of primary particle
THETAP 0. 89.                 range of zenith angle (degree)
PHIP   0. 360.                range of azimuth angle (degree)
SEED   107  0  0              seed for 1. random number sequence
SEED   108  0  0              seed for 2. random number sequence
OBSLEV 110.E2                 observation level (in cm)
FIXCHI 0.                     starting altitude (g/cm**2)
MAGNET 20.0 42.8              magnetic field centr. Europe
HADFLG 0 0 0 0 0 2            flags hadr.interact.&fragmentation
ECUTS  9.E0 9.E0 1.E6 1.E6    energy cuts for particles
MUADDI T                      additional info for muons
MUMULT T                      muon multiple scattering angle
ELMFLG F  F                   em. interaction flags (NKG,EGS)
STEPFC 1.0                    mult. scattering step length fact.
RADNKG 200.E2                 outer radius for NKG lat.dens.distr.
ARRANG 0.                     rotation of array to north
LONGI  F 20. T F              longit.distr. & step size & fit & out
ECTMAP 1.E3                   cut on gamma factor for printout
MAXPRT 100                    max. number of printed events
DIRECT /home/ochillo/data/qgs/      output directory
DATBAS T                      write .dbase file
USER   you                    user
DEBUG  F 6 F 1000000          debug flag and log.unit for out
EXIT                          terminates input
```

Note: T ≡ True F ≡ False

APPENDIX II
VALUES OF SIMULATED MUON CHARGE RATIO

Zenith angle 0° – 10°		10° – 20°		20° – 30°	
Azimuth (°)	Charge ratio	Charge ratio		Charge ratio	
5	1.125596 +- 0.1101428E-01	1.131966	+- 0.6529896E-02	1.142679	+- 0.5438947E-02
15	1.148169 +- 0.1124714E-01	1.129790	+- 0.6562808E-02	1.147706	+- 0.5471186E-02
25	1.148292 +- 0.1131559E-01	1.128065	+- 0.6573814E-02	1.141963	+- 0.5441825E-02
35	1.129580 +- 0.1117286E-01	1.134670	+- 0.6608075E-02	1.128010	+- 0.5372200E-02
45	1.153283 +- 0.1135361E-01	1.139920	+- 0.6609478E-02	1.142630	+- 0.5456794E-02
55	1.126376 +- 0.1094654E-01	1.129554	+- 0.6588585E-02	1.133218	+- 0.5403661E-02
65	1.155573 +- 0.1127188E-01	1.136225	+- 0.6602464E-02	1.136351	+- 0.5397748E-02
75	1.126775 +- 0.1096460E-01	1.142449	+- 0.6633318E-02	1.148257	+- 0.5475529E-02
85	1.136758 +- 0.1110426E-01	1.142946	+- 0.6604321E-02	1.137587	+- 0.5431462E-02
95	1.141523 +- 0.1116772E-01	1.139747	+- 0.6621172E-02	1.139993	+- 0.5406719E-02
105	1.131400 +- 0.1106725E-01	1.127331	+- 0.6576702E-02	1.146391	+- 0.5442208E-02
115	1.148644 +- 0.1131384E-01	1.127678	+- 0.6542420E-02	1.141988	+- 0.5433373E-02
125	1.125371 +- 0.1105867E-01	1.133309	+- 0.6600460E-02	1.136990	+- 0.5401792E-02
135	1.120188 +- 0.1094691E-01	1.135525	+- 0.6611652E-02	1.141622	+- 0.5425037E-02
145	1.147334 +- 0.1122275E-01	1.136414	+- 0.6617044E-02	1.135395	+- 0.5411410E-02
155	1.117005 +- 0.1093473E-01	1.135087	+- 0.6595917E-02	1.136410	+- 0.5385183E-02
165	1.140444 +- 0.1121238E-01	1.138085	+- 0.6587887E-02	1.135718	+- 0.5392179E-02
175	1.145604 +- 0.1130171E-01	1.123771	+- 0.6526007E-02	1.126380	+- 0.5352121E-02
185	1.149341 +- 0.1127505E-01	1.145325	+- 0.6641999E-02	1.136664	+- 0.5403430E-02
195	1.147935 +- 0.1125404E-01	1.136055	+- 0.6633532E-02	1.137454	+- 0.5433382E-02
205	1.138220 +- 0.1114551E-01	1.138477	+- 0.6635949E-02	1.134682	+- 0.5396245E-02
215	1.143183 +- 0.1115148E-01	1.138684	+- 0.6594191E-02	1.142642	+- 0.5452431E-02
225	1.133381 +- 0.1109053E-01	1.138327	+- 0.6637320E-02	1.137154	+- 0.5417503E-02
235	1.155758 +- 0.1128739E-01	1.138358	+- 0.6618736E-02	1.138794	+- 0.5424865E-02
245	1.149521 +- 0.1122339E-01	1.141028	+- 0.6628660E-02	1.128808	+- 0.5387787E-02
255	1.125454 +- 0.1098929E-01	1.149397	+- 0.6645689E-02	1.141600	+- 0.5443763E-02
265	1.126639 +- 0.1103440E-01	1.134648	+- 0.6616751E-02	1.130920	+- 0.5378115E-02
275	1.137893 +- 0.1126592E-01	1.146029	+- 0.6695204E-02	1.131375	+- 0.5390100E-02
285	1.148669 +- 0.1131697E-01	1.139231	+- 0.6640454E-02	1.145565	+- 0.5449444E-02
295	1.154703 +- 0.1132707E-01	1.145482	+- 0.6666923E-02	1.145877	+- 0.5442664E-02
305	1.153755 +- 0.1132489E-01	1.144498	+- 0.6662771E-02	1.145020	+- 0.5432510E-02
315	1.122682 +- 0.1089947E-01	1.137136	+- 0.6591735E-02	1.133821	+- 0.5397330E-02
325	1.136528 +- 0.1110761E-01	1.133380	+- 0.6577231E-02	1.141909	+- 0.5436662E-02
335	1.118977 +- 0.1101287E-01	1.141992	+- 0.6661106E-02	1.132070	+- 0.5403157E-02
345	1.126298 +- 0.1103914E-01	1.145446	+- 0.6650245E-02	1.133657	+- 0.5417842E-02
355	1.143089 +- 0.1113524E-01	1.128952	+- 0.6565076E-02	1.135913	+- 0.5400112E-02

Table A2.1: Values of simulated muon charge ratio at different azimuth angles, with the zenith angles taken at intervals of 10° from 0° to 30° using the QGSJET II model.

	Zenith angle 30° – 40°		40° – 50°		50° – 60°	
Azimuth (°)	Charge ratio		Charge ratio		Charge ratio	
5	1.141647	+- 0.5007794E-02	1.141072	+- 0.5062677E-02	1.135185	+- 0.5604151E-02
15	1.145279	+- 0.5044486E-02	1.130186	+- 0.5013795E-02	1.145904	+- 0.5651515E-02
25	1.144003	+- 0.5047393E-02	1.142066	+- 0.5065074E-02	1.136750	+- 0.5590975E-02
35	1.134025	+- 0.4990742E-02	1.141485	+- 0.5078862E-02	1.128153	+- 0.5526490E-02
45	1.135082	+- 0.4998239E-02	1.142800	+- 0.5058851E-02	1.121209	+- 0.5510914E-02
55	1.139651	+- 0.5026512E-02	1.142743	+- 0.5073817E-02	1.138347	+- 0.5613234E-02
65	1.130273	+- 0.4944899E-02	1.141150	+- 0.5073600E-02	1.136431	+- 0.5557435E-02
75	1.144811	+- 0.5021007E-02	1.139052	+- 0.5061037E-02	1.143018	+- 0.5606045E-02
85	1.135918	+- 0.4993317E-02	1.145295	+- 0.5084482E-02	1.147481	+- 0.5645905E-02
95	1.147103	+- 0.5066016E-02	1.131267	+- 0.5013985E-02	1.151225	+- 0.5661354E-02
105	1.140752	+- 0.5039745E-02	1.140666	+- 0.5076712E-02	1.149929	+- 0.5632169E-02
115	1.146327	+- 0.5070711E-02	1.137649	+- 0.5058495E-02	1.131510	+- 0.5565467E-02
125	1.137769	+- 0.5015892E-02	1.142821	+- 0.5055594E-02	1.143032	+- 0.5617966E-02
135	1.141424	+- 0.5024987E-02	1.140190	+- 0.5087346E-02	1.146945	+- 0.5648013E-02
145	1.145378	+- 0.5028468E-02	1.140234	+- 0.5081947E-02	1.145859	+- 0.5635703E-02
155	1.134175	+- 0.4994615E-02	1.142213	+- 0.5066688E-02	1.165640	+- 0.5728471E-02
165	1.145916	+- 0.5036190E-02	1.156543	+- 0.5157724E-02	1.163135	+- 0.5715660E-02
175	1.143458	+- 0.5027671E-02	1.139612	+- 0.5054267E-02	1.146196	+- 0.5618640E-02
185	1.136447	+- 0.4995203E-02	1.131960	+- 0.5011689E-02	1.156269	+- 0.5699713E-02
195	1.126090	+- 0.4973552E-02	1.137651	+- 0.5061245E-02	1.148889	+- 0.5643597E-02
205	1.134775	+- 0.4994580E-02	1.143444	+- 0.5085648E-02	1.147962	+- 0.5656436E-02
215	1.132202	+- 0.4971617E-02	1.139991	+- 0.5080741E-02	1.142266	+- 0.5598262E-02
225	1.145605	+- 0.5042976E-02	1.151202	+- 0.5124307E-02	1.149631	+- 0.5634631E-02
235	1.135524	+- 0.4969748E-02	1.141230	+- 0.5069254E-02	1.148775	+- 0.5645172E-02
245	1.135327	+- 0.5010104E-02	1.142823	+- 0.5073448E-02	1.148108	+- 0.5639780E-02
255	1.143314	+- 0.5051415E-02	1.140626	+- 0.5077193E-02	1.151344	+- 0.5671794E-02
265	1.140644	+- 0.5023729E-02	1.142976	+- 0.5080249E-02	1.142462	+- 0.5609931E-02
275	1.143705	+- 0.5049562E-02	1.149050	+- 0.5091324E-02	1.155748	+- 0.5701568E-02
285	1.137484	+- 0.5005979E-02	1.139026	+- 0.5066224E-02	1.143504	+- 0.5590610E-02
295	1.146973	+- 0.5056550E-02	1.132380	+- 0.5011599E-02	1.131729	+- 0.5565508E-02
305	1.137361	+- 0.4983373E-02	1.138190	+- 0.5055421E-02	1.151390	+- 0.5658538E-02
315	1.151136	+- 0.5078649E-02	1.139981	+- 0.5057825E-02	1.144433	+- 0.5617929E-02
325	1.128909	+- 0.4968133E-02	1.135562	+- 0.5071032E-02	1.135754	+- 0.5593490E-02
335	1.137851	+- 0.5019907E-02	1.152033	+- 0.5117768E-02	1.136101	+- 0.5593967E-02
345	1.138333	+- 0.5015825E-02	1.141904	+- 0.5050637E-02	1.144051	+- 0.5616816E-02
355	1.132336	+- 0.4978649E-02	1.141947	+- 0.5058625E-02	1.140636	+- 0.5583419E-02

Table A2.2: Values of simulated muon charge ratio at different azimuth angles, with the zenith angles taken at intervals of 10° from 30° to 60° using the QGSJET II model.

	Zenith angle 60° – 70°		70° – 80°		80° – 89°	
Azimuth (°)	Charge ratio		Charge ratio		Charge ratio	
5	1.135170	+- 0.6979777E-02	1.111010	+- 0.1090839E-01	0.851963	+- 0.2428648E-01
15	1.138280	+- 0.7027550E-02	1.085420	+- 0.1068994E-01	0.854503	+- 0.2496303E-01
25	1.115943	+- 0.6872765E-02	1.103781	+- 0.1094426E-01	0.850853	+- 0.2499348E-01
35	1.130740	+- 0.6979635E-02	1.117819	+- 0.1092702E-01	0.888405	+- 0.2576621E-01
45	1.133249	+- 0.6982526E-02	1.120077	+- 0.1097798E-01	0.980587	+- 0.2832321E-01
55	1.125403	+- 0.6943266E-02	1.111190	+- 0.1087641E-01	0.951802	+- 0.2743031E-01
65	1.148739	+- 0.7083978E-02	1.132525	+- 0.1109513E-01	1.106826	+- 0.3215026E-01
75	1.151003	+- 0.7094405E-02	1.152085	+- 0.1125638E-01	1.178241	+- 0.3447014E-01
85	1.141920	+- 0.7014445E-02	1.154284	+- 0.1139048E-01	1.153258	+- 0.3340768E-01
95	1.148127	+- 0.7072320E-02	1.185576	+- 0.1163680E-01	1.192360	+- 0.3447840E-01
105	1.164201	+- 0.7185871E-02	1.158914	+- 0.1139705E-01	1.233165	+- 0.3551765E-01
115	1.164696	+- 0.7139156E-02	1.189804	+- 0.1162393E-01	1.354136	+- 0.3973550E-01
125	1.163514	+- 0.7155534E-02	1.208698	+- 0.1186297E-01	1.368737	+- 0.4030308E-01
135	1.162404	+- 0.7163044E-02	1.195529	+- 0.1172223E-01	1.405222	+- 0.4201125E-01
145	1.175275	+- 0.7215826E-02	1.235428	+- 0.1209707E-01	1.683552	+- 0.5188864E-01
155	1.158436	+- 0.7155133E-02	1.230409	+- 0.1209131E-01	1.657596	+- 0.4997291E-01
165	1.179547	+- 0.7294496E-02	1.270748	+- 0.1258082E-01	1.683400	+- 0.5076278E-01
175	1.175909	+- 0.7253403E-02	1.242831	+- 0.1225770E-01	1.650365	+- 0.4958553E-01
185	1.158242	+- 0.7120902E-02	1.254464	+- 0.1242714E-01	1.649496	+- 0.4946711E-01
195	1.171471	+- 0.7229340E-02	1.232355	+- 0.1220241E-01	1.627176	+- 0.4899253E-01
205	1.179047	+- 0.7301338E-02	1.215741	+- 0.1201759E-01	1.689715	+- 0.5138892E-01
215	1.166007	+- 0.7194963E-02	1.251432	+- 0.1245865E-01	1.500797	+- 0.4466897E-01
225	1.166003	+- 0.7179801E-02	1.222646	+- 0.1208177E-01	1.443709	+- 0.4239399E-01
235	1.157320	+- 0.7144501E-02	1.248352	+- 0.1231528E-01	1.403218	+- 0.4117577E-01
245	1.164786	+- 0.7167526E-02	1.180041	+- 0.1158158E-01	1.345716	+- 0.3954087E-01
255	1.154875	+- 0.7112938E-02	1.178921	+- 0.1153708E-01	1.251514	+- 0.3622756E-01
265	1.148502	+- 0.7070935E-02	1.159220	+- 0.1122841E-01	1.214419	+- 0.3548246E-01
275	1.141780	+- 0.6984132E-02	1.147377	+- 0.1129548E-01	1.105705	+- 0.3208989E-01
285	1.136163	+- 0.6989300E-02	1.145548	+- 0.1120162E-01	1.088640	+- 0.3127922E-01
295	1.139780	+- 0.7049966E-02	1.087319	+- 0.1060530E-01	1.138965	+- 0.3326199E-01
305	1.145391	+- 0.7086168E-02	1.111724	+- 0.1095383E-01	0.983229	+- 0.2859364E-01
315	1.135516	+- 0.6994492E-02	1.100005	+- 0.1072330E-01	0.989418	+- 0.2830416E-01
325	1.121880	+- 0.6905657E-02	1.092303	+- 0.1073659E-01	0.846966	+- 0.2428252E-01
335	1.142193	+- 0.7093715E-02	1.077475	+- 0.1056056E-01	0.910729	+- 0.2639355E-01
345	1.132113	+- 0.6984989E-02	1.100541	+- 0.1081266E-01	0.863195	+- 0.2500136E-01
355	1.122717	+- 0.6877570E-02	1.104531	+- 0.1078244E-01	0.824942	+- 0.2414672E-01

Table A2.3: Values of simulated muon charge ratio at different azimuth angles, with the zenith angles taken at intervals of 10° from 60° to 89° using the QGSJET II model.

Zenith angle 0° – 10°		10° – 20°		20° – 30°	
Azimuth (°)	Charge ratio	Charge ratio		Charge ratio	
5	1.332739 +- 0.1191961E-01	1.329676	+- 0.7018490E-02	1.347271	+- 0.5842398E-02
15	1.340834 +- 0.1198141E-01	1.336555	+- 0.7034151E-02	1.338649	+- 0.5794079E-02
25	1.343622 +- 0.1202661E-01	1.335904	+- 0.7051767E-02	1.348718	+- 0.5839210E-02
35	1.335569 +- 0.1188934E-01	1.348052	+- 0.7080352E-02	1.347370	+- 0.5832513E-02
45	1.332764 +- 0.1182399E-01	1.346046	+- 0.7097170E-02	1.337498	+- 0.5770734E-02
55	1.332685 +- 0.1185574E-01	1.346974	+- 0.7107257E-02	1.332615	+- 0.5756533E-02
65	1.316604 +- 0.1165978E-01	1.329087	+- 0.7011980E-02	1.342546	+- 0.5798860E-02
75	1.332225 +- 0.1181466E-01	1.340274	+- 0.7058376E-02	1.336041	+- 0.5764534E-02
85	1.343727 +- 0.1194722E-01	1.338503	+- 0.7038084E-02	1.343151	+- 0.5784855E-02
95	1.344034 +- 0.1194369E-01	1.342043	+- 0.7067889E-02	1.337284	+- 0.5793009E-02
105	1.348286 +- 0.1198345E-01	1.337815	+- 0.7070856E-02	1.352098	+- 0.5856373E-02
115	1.336627 +- 0.1187149E-01	1.344734	+- 0.7095463E-02	1.342006	+- 0.5781896E-02
125	1.317935 +- 0.1171664E-01	1.340671	+- 0.7064789E-02	1.342567	+- 0.5785400E-02
135	1.336759 +- 0.1186518E-01	1.342939	+- 0.7097194E-02	1.341631	+- 0.5789717E-02
145	1.340672 +- 0.1192315E-01	1.334021	+- 0.7030691E-02	1.337383	+- 0.5766721E-02
155	1.348866 +- 0.1202493E-01	1.333381	+- 0.7001687E-02	1.337926	+- 0.5778037E-02
165	1.337045 +- 0.1191778E-01	1.347518	+- 0.7093721E-02	1.340271	+- 0.5761086E-02
175	1.345463 +- 0.1196587E-01	1.354736	+- 0.7137204E-02	1.331672	+- 0.5744245E-02
185	1.343060 +- 0.1193175E-01	1.328331	+- 0.6985972E-02	1.345162	+- 0.5808522E-02
195	1.343338 +- 0.1192829E-01	1.336161	+- 0.7068110E-02	1.337298	+- 0.5748420E-02
205	1.334196 +- 0.1179032E-01	1.344771	+- 0.7117127E-02	1.337221	+- 0.5754187E-02
215	1.350210 +- 0.1198252E-01	1.332216	+- 0.6994070E-02	1.338450	+- 0.5748456E-02
225	1.323477 +- 0.1175554E-01	1.328455	+- 0.6991837E-02	1.342707	+- 0.5780861E-02
235	1.348709 +- 0.1203371E-01	1.324895	+- 0.6952772E-02	1.337522	+- 0.5772289E-02
245	1.336528 +- 0.1185396E-01	1.338761	+- 0.7055863E-02	1.330187	+- 0.5730208E-02
255	1.344055 +- 0.1195520E-01	1.345410	+- 0.7112307E-02	1.339276	+- 0.5783018E-02
265	1.312511 +- 0.1161248E-01	1.342442	+- 0.7072183E-02	1.342007	+- 0.5802708E-02
275	1.338083 +- 0.1193373E-01	1.345193	+- 0.7102587E-02	1.338857	+- 0.5786233E-02
285	1.323523 +- 0.1175507E-01	1.343410	+- 0.7060658E-02	1.345257	+- 0.5836564E-02
295	1.352997 +- 0.1203334E-01	1.337302	+- 0.7029670E-02	1.342719	+- 0.5786745E-02
305	1.345777 +- 0.1194452E-01	1.330467	+- 0.7046688E-02	1.347918	+- 0.5825835E-02
315	1.326238 +- 0.1180774E-01	1.338335	+- 0.7053147E-02	1.344092	+- 0.5794175E-02
325	1.315201 +- 0.1169522E-01	1.345617	+- 0.7076004E-02	1.343762	+- 0.5815096E-02
335	1.326734 +- 0.1178593E-01	1.333016	+- 0.7026638E-02	1.345679	+- 0.5786195E-02
345	1.353210 +- 0.1207195E-01	1.332291	+- 0.6986907E-02	1.331596	+- 0.5728849E-02
355	1.323922 +- 0.1185602E-01	1.341505	+- 0.7057476E-02	1.343058	+- 0.5818103E-02

Table A2.4: Values of simulated muon charge ratio at different azimuth angles, with the zenith angles taken at intervals of 10° from 0° to 30° using the SIBYLL model.

	Zenith angle 30° – 40°		40° – 50°		50° – 60°	
Azimuth (°)	Charge ratio		Charge ratio		Charge ratio	
5	1.338655	+- 0.5341225E-02	1.347271	+- 0.5842398E-02	1.354370	+- 0.6022605E-02
15	1.346174	+- 0.5363123E-02	1.338649	+- 0.5794079E-02	1.351640	+- 0.6014994E-02
25	1.344628	+- 0.5372433E-02	1.348718	+- 0.5839210E-02	1.350025	+- 0.6016287E-02
35	1.336244	+- 0.5342676E-02	1.347370	+- 0.5832513E-02	1.347550	+- 0.5999057E-02
45	1.343107	+- 0.5382605E-02	1.337498	+- 0.5770734E-02	1.353171	+- 0.6025159E-02
55	1.354296	+- 0.5423387E-02	1.332615	+- 0.5756533E-02	1.350379	+- 0.6031206E-02
65	1.348516	+- 0.5377717E-02	1.342546	+- 0.5798860E-02	1.363001	+- 0.6072445E-02
75	1.345128	+- 0.5392900E-02	1.336041	+- 0.5764534E-02	1.356167	+- 0.6070822E-02
85	1.343805	+- 0.5372578E-02	1.343151	+- 0.5784855E-02	1.356829	+- 0.6066828E-02
95	1.347050	+- 0.5396126E-02	1.337284	+- 0.5793009E-02	1.359397	+- 0.6040588E-02
105	1.350689	+- 0.5407746E-02	1.352098	+- 0.5856373E-02	1.361785	+- 0.6064978E-02
115	1.343012	+- 0.5355965E-02	1.342006	+- 0.5781896E-02	1.369777	+- 0.6119195E-02
125	1.348487	+- 0.5400235E-02	1.342567	+- 0.5785400E-02	1.375855	+- 0.6130545E-02
135	1.347645	+- 0.5415285E-02	1.341631	+- 0.5789717E-02	1.368239	+- 0.6077667E-02
145	1.348368	+- 0.5370904E-02	1.337383	+- 0.5766721E-02	1.362472	+- 0.6083449E-02
155	1.346262	+- 0.5384946E-02	1.337926	+- 0.5778037E-02	1.372357	+- 0.6127013E-02
165	1.336807	+- 0.5339200E-02	1.340271	+- 0.5761086E-02	1.362025	+- 0.6088951E-02
175	1.356260	+- 0.5448513E-02	1.331672	+- 0.5744245E-02	1.364748	+- 0.6070732E-02
185	1.349731	+- 0.5397202E-02	1.345162	+- 0.5808522E-02	1.366646	+- 0.6094987E-02
195	1.336191	+- 0.5341215E-02	1.337298	+- 0.5748420E-02	1.364661	+- 0.6078935E-02
205	1.344807	+- 0.5382912E-02	1.337221	+- 0.5754187E-02	1.371105	+- 0.6098252E-02
215	1.347290	+- 0.5398672E-02	1.338450	+- 0.5748456E-02	1.360295	+- 0.6077115E-02
225	1.354155	+- 0.5416227E-02	1.342707	+- 0.5780861E-02	1.374032	+- 0.6125119E-02
235	1.340795	+- 0.5368204E-02	1.337522	+- 0.5772289E-02	1.361207	+- 0.6067323E-02
245	1.339463	+- 0.5363640E-02	1.330187	+- 0.5730208E-02	1.366027	+- 0.6113383E-02
255	1.350259	+- 0.5411752E-02	1.339276	+- 0.5783018E-02	1.354737	+- 0.6032336E-02
265	1.329204	+- 0.5298959E-02	1.342007	+- 0.5802708E-02	1.367711	+- 0.6083902E-02
275	1.346768	+- 0.5390324E-02	1.338857	+- 0.5786233E-02	1.352680	+- 0.6015077E-02
285	1.347107	+- 0.5380988E-02	1.345257	+- 0.5836564E-02	1.366936	+- 0.6108862E-02
295	1.355410	+- 0.5416918E-02	1.342719	+- 0.5786745E-02	1.358092	+- 0.6051251E-02
305	1.352221	+- 0.5399488E-02	1.347918	+- 0.5825835E-02	1.355488	+- 0.6039416E-02
315	1.347909	+- 0.5406734E-02	1.344092	+- 0.5794175E-02	1.350799	+- 0.6012938E-02
325	1.349632	+- 0.5402723E-02	1.343762	+- 0.5815096E-02	1.357978	+- 0.6070177E-02
335	1.344966	+- 0.5382571E-02	1.345679	+- 0.5786195E-02	1.352033	+- 0.6045619E-02
345	1.351790	+- 0.5415160E-02	1.331596	+- 0.5728849E-02	1.344976	+- 0.6012861E-02
355	1.356876	+- 0.5427995E-02	1.343058	+- 0.5818103E-02	1.357016	+- 0.6058532E-02

Table A2.5: Values of simulated muon charge ratio at different azimuth angles, with the zenith angles taken at intervals of 10° from 30° to 60° using the SIBYLL model.

Zenith angle	60° – 70°		70° – 80°		80° – 89°	
Azimuth (°)	Charge ratio		Charge ratio		Charge ratio	
5	1.337546	+- 0.7481286E-02	1.319580	+- 0.1172285E-01	1.068832	+- 0.2793791E-01
15	1.333268	+- 0.7470500E-02	1.312300	+- 0.1159969E-01	1.030426	+- 0.2659518E-01
25	1.357920	+- 0.7632562E-02	1.307845	+- 0.1154020E-01	1.120014	+- 0.2907921E-01
35	1.348322	+- 0.7540475E-02	1.352250	+- 0.1201690E-01	1.111267	+- 0.2865165E-01
45	1.353458	+- 0.7541847E-02	1.352134	+- 0.1188463E-01	1.149758	+- 0.2920444E-01
55	1.351009	+- 0.7510273E-02	1.342696	+- 0.1185198E-01	1.213348	+- 0.3087621E-01
65	1.356857	+- 0.7545318E-02	1.348157	+- 0.1197332E-01	1.260695	+- 0.3228102E-01
75	1.363953	+- 0.7623643E-02	1.384542	+- 0.1227704E-01	1.284145	+- 0.3277238E-01
85	1.373540	+- 0.7670868E-02	1.384884	+- 0.1223706E-01	1.437074	+- 0.3643648E-01
95	1.383694	+- 0.7735402E-02	1.403242	+- 0.1228801E-01	1.393066	+- 0.3603713E-01
105	1.383205	+- 0.7738929E-02	1.408360	+- 0.1248212E-01	1.557137	+- 0.4024030E-01
115	1.386084	+- 0.7739361E-02	1.438465	+- 0.1275124E-01	1.626748	+- 0.4321568E-01
125	1.398497	+- 0.7840851E-02	1.483179	+- 0.1324756E-01	1.655852	+- 0.4249749E-01
135	1.397156	+- 0.7804489E-02	1.474715	+- 0.1300020E-01	1.752527	+- 0.4604766E-01
145	1.401120	+- 0.7846955E-02	1.490103	+- 0.1323935E-01	1.899439	+- 0.5075347E-01
155	1.385404	+- 0.7735169E-02	1.485015	+- 0.1320789E-01	1.890796	+- 0.5105425E-01
165	1.412668	+- 0.7905676E-02	1.515061	+- 0.1343396E-01	2.047666	+- 0.5566517E-01
175	1.398917	+- 0.7809222E-02	1.495875	+- 0.1322949E-01	2.112662	+- 0.5829622E-01
185	1.393305	+- 0.7792924E-02	1.506392	+- 0.1347033E-01	1.984321	+- 0.5386508E-01
195	1.404530	+- 0.7851306E-02	1.527838	+- 0.1359735E-01	1.921540	+- 0.5230485E-01
205	1.392356	+- 0.7782559E-02	1.481928	+- 0.1313946E-01	1.957698	+- 0.5336802E-01
215	1.388167	+- 0.7750732E-02	1.467987	+- 0.1310331E-01	1.778710	+- 0.4672357E-01
225	1.391931	+- 0.7796008E-02	1.473266	+- 0.1312472E-01	1.816040	+- 0.4813721E-01
235	1.398459	+- 0.7817147E-02	1.472579	+- 0.1315439E-01	1.734852	+- 0.4515438E-01
245	1.379596	+- 0.7720446E-02	1.423040	+- 0.1259242E-01	1.612202	+- 0.4195095E-01
255	1.376461	+- 0.7687212E-02	1.422108	+- 0.1248409E-01	1.621577	+- 0.4199925E-01
265	1.371349	+- 0.7654992E-02	1.397013	+- 0.1232845E-01	1.477470	+- 0.3803675E-01
275	1.367120	+- 0.7649953E-02	1.397196	+- 0.1230796E-01	1.470660	+- 0.3847914E-01
285	1.365291	+- 0.7639392E-02	1.376103	+- 0.1216277E-01	1.345475	+- 0.3442450E-01
295	1.369348	+- 0.7669777E-02	1.365217	+- 0.1213907E-01	1.286251	+- 0.3323692E-01
305	1.356429	+- 0.7554950E-02	1.330280	+- 0.1171200E-01	1.200500	+- 0.3072685E-01
315	1.347952	+- 0.7519158E-02	1.317806	+- 0.1159114E-01	1.197420	+- 0.3070435E-01
325	1.332269	+- 0.7422623E-02	1.326403	+- 0.1173331E-01	1.105139	+- 0.2804462E-01
335	1.347879	+- 0.7571294E-02	1.336286	+- 0.1181802E-01	1.057809	+- 0.2712734E-01
345	1.364970	+- 0.7642953E-02	1.303649	+- 0.1149776E-01	1.031719	+- 0.2673810E-01
355	1.339036	+- 0.7462894E-02	1.299155	+- 0.1143805E-01	1.029727	+- 0.2687854E-01

Table A2.6: Values of simulated muon charge ratio at different azimuth angles, with the zenith angles taken at intervals of 10° from 60° to 89° using the SIBYLL model.

Zenith angle 0° – 10°		10° – 20°		20° – 30°	
Azimuth (°)	Charge ratio	Charge ratio		Charge ratio	
5	1.208150	+- 0.1123023E-01	1.215466	+- 0.6724548E-02	1.212865	+- 0.5488574E-02
15	1.199133	+- 0.1114721E-01	1.208381	+- 0.6670876E-02	1.200491	+- 0.5419727E-02
25	1.212137	+- 0.1128829E-01	1.215825	+- 0.6720951E-02	1.210151	+- 0.5469313E-02
35	1.203054	+- 0.1115882E-01	1.204074	+- 0.6654033E-02	1.204616	+- 0.5423211E-02
45	1.195120	+- 0.1113835E-01	1.212380	+- 0.6662062E-02	1.203289	+- 0.5432687E-02
55	1.208073	+- 0.1132838E-01	1.212002	+- 0.6690577E-02	1.213152	+- 0.5477848E-02
65	1.202768	+- 0.1122447E-01	1.207893	+- 0.6656978E-02	1.220567	+- 0.5553292E-02
75	1.198534	+- 0.1120058E-01	1.220536	+- 0.6730628E-02	1.208677	+- 0.5490442E-02
85	1.223910	+- 0.1136799E-01	1.203305	+- 0.6622798E-02	1.208930	+- 0.5477649E-02
95	1.200732	+- 0.1120739E-01	1.218508	+- 0.6714952E-02	1.220882	+- 0.5517672E-02
105	1.185322	+- 0.1100734E-01	1.204050	+- 0.6669919E-02	1.208484	+- 0.5454130E-02
115	1.209402	+- 0.1115206E-01	1.218467	+- 0.6720047E-02	1.215096	+- 0.5478369E-02
125	1.206602	+- 0.1118111E-01	1.210705	+- 0.6695218E-02	1.204963	+- 0.5474237E-02
135	1.183387	+- 0.1100842E-01	1.202029	+- 0.6624660E-02	1.208405	+- 0.5483392E-02
145	1.225879	+- 0.1139949E-01	1.207322	+- 0.6638239E-02	1.217819	+- 0.5506976E-02
155	1.206266	+- 0.1115568E-01	1.205735	+- 0.6620607E-02	1.211544	+- 0.5467188E-02
165	1.215956	+- 0.1138665E-01	1.205562	+- 0.6662056E-02	1.206782	+- 0.5448520E-02
175	1.187777	+- 0.1113430E-01	1.219096	+- 0.6771096E-02	1.209977	+- 0.5504810E-02
185	1.181381	+- 0.1097449E-01	1.207950	+- 0.6676831E-02	1.212117	+- 0.5475730E-02
195	1.203220	+- 0.1123763E-01	1.210706	+- 0.6699769E-02	1.210496	+- 0.5483631E-02
205	1.220516	+- 0.1138471E-01	1.204498	+- 0.6655956E-02	1.219851	+- 0.5519578E-02
215	1.214360	+- 0.1130028E-01	1.211626	+- 0.6719389E-02	1.203746	+- 0.5466049E-02
225	1.210099	+- 0.1119802E-01	1.214407	+- 0.6716570E-02	1.212385	+- 0.5519106E-02
235	1.215375	+- 0.1131055E-01	1.208231	+- 0.6639472E-02	1.224922	+- 0.5532748E-02
245	1.184564	+- 0.1104227E-01	1.206760	+- 0.6653694E-02	1.207222	+- 0.5454527E-02
255	1.209442	+- 0.1122599E-01	1.213266	+- 0.6714335E-02	1.202743	+- 0.5432566E-02
265	1.226459	+- 0.1143038E-01	1.212251	+- 0.6706947E-02	1.211797	+- 0.5484370E-02
275	1.212857	+- 0.1126727E-01	1.219374	+- 0.6769251E-02	1.213467	+- 0.5494383E-02
285	1.202633	+- 0.1118052E-01	1.219591	+- 0.6732615E-02	1.206457	+- 0.5477910E-02
295	1.206230	+- 0.1119897E-01	1.213342	+- 0.6703188E-02	1.217227	+- 0.5534905E-02
305	1.206037	+- 0.1123737E-01	1.214867	+- 0.6739204E-02	1.217422	+- 0.5511217E-02
315	1.222737	+- 0.1139885E-01	1.211301	+- 0.6723547E-02	1.213753	+- 0.5467923E-02
325	1.213769	+- 0.1134978E-01	1.203593	+- 0.6667067E-02	1.205057	+- 0.5441494E-02
335	1.224472	+- 0.1140566E-01	1.193247	+- 0.6608919E-02	1.199327	+- 0.5419343E-02
345	1.220834	+- 0.1136935E-01	1.218601	+- 0.6730410E-02	1.207774	+- 0.5458863E-02
355	1.201034	+- 0.1119547E-01	1.201491	+- 0.6626047E-02	1.213045	+- 0.5504020E-02

Table A2.7: Values of simulated muon charge ratio at different azimuth angles, with the zenith angles taken at intervals of 10° from 0° to 30° using the VENUS model.

Zenith angle 30° – 40°		40° – 50°		50° – 60°	
Azimuth (°)	Charge ratio		Charge ratio		Charge ratio
5	1.206707	+- 0.5052039E-02	1.212156	+- 0.5126326E-02	1.222354	+- 0.5736391E-02
15	1.214432	+- 0.5087052E-02	1.229083	+- 0.5210561E-02	1.210269	+- 0.5636107E-02
25	1.208290	+- 0.5056946E-02	1.213976	+- 0.5122752E-02	1.205374	+- 0.5610975E-02
35	1.211505	+- 0.5080541E-02	1.222185	+- 0.5196324E-02	1.212932	+- 0.5666160E-02
45	1.205482	+- 0.5046210E-02	1.213177	+- 0.5125100E-02	1.216121	+- 0.5694502E-02
55	1.202609	+- 0.5018916E-02	1.209835	+- 0.5120534E-02	1.223124	+- 0.5738182E-02
65	1.214153	+- 0.5086147E-02	1.211020	+- 0.5143443E-02	1.220196	+- 0.5714849E-02
75	1.198253	+- 0.5011585E-02	1.214722	+- 0.5154614E-02	1.219333	+- 0.5674015E-02
85	1.210130	+- 0.5074244E-02	1.207427	+- 0.5106318E-02	1.227365	+- 0.5717371E-02
95	1.211991	+- 0.5055933E-02	1.217792	+- 0.5137275E-02	1.223848	+- 0.5729171E-02
105	1.213127	+- 0.5083553E-02	1.208557	+- 0.5118483E-02	1.222546	+- 0.5716558E-02
115	1.218274	+- 0.5122633E-02	1.218918	+- 0.5159668E-02	1.220240	+- 0.5701553E-02
125	1.210025	+- 0.5063145E-02	1.211254	+- 0.5125987E-02	1.223956	+- 0.5731569E-02
135	1.217598	+- 0.5091810E-02	1.220624	+- 0.5162188E-02	1.235893	+- 0.5809486E-02
145	1.211209	+- 0.5056710E-02	1.216703	+- 0.5144815E-02	1.227139	+- 0.5751178E-02
155	1.212816	+- 0.5072763E-02	1.215875	+- 0.5116880E-02	1.230785	+- 0.5759796E-02
165	1.212849	+- 0.5058703E-02	1.223051	+- 0.5173551E-02	1.222829	+- 0.5701392E-02
175	1.208421	+- 0.5051298E-02	1.212857	+- 0.5137085E-02	1.233262	+- 0.5749612E-02
185	1.217801	+- 0.5106114E-02	1.215062	+- 0.5132969E-02	1.238571	+- 0.5790019E-02
195	1.211508	+- 0.5088942E-02	1.220484	+- 0.5182301E-02	1.231136	+- 0.5757315E-02
205	1.207141	+- 0.5047521E-02	1.215657	+- 0.5125241E-02	1.240796	+- 0.5834541E-02
215	1.208541	+- 0.5066287E-02	1.221258	+- 0.5145156E-02	1.234844	+- 0.5740506E-02
225	1.208593	+- 0.5087069E-02	1.210582	+- 0.5122052E-02	1.227960	+- 0.5764253E-02
235	1.207733	+- 0.5053954E-02	1.224422	+- 0.5184094E-02	1.223515	+- 0.5742771E-02
245	1.215346	+- 0.5099594E-02	1.213015	+- 0.5141650E-02	1.233330	+- 0.5781870E-02
255	1.212603	+- 0.5070228E-02	1.227480	+- 0.5208155E-02	1.234439	+- 0.5775049E-02
265	1.218044	+- 0.5116793E-02	1.219771	+- 0.5153317E-02	1.219347	+- 0.5704655E-02
275	1.208924	+- 0.5068551E-02	1.214493	+- 0.5109918E-02	1.223219	+- 0.5721922E-02
285	1.215380	+- 0.5100567E-02	1.219197	+- 0.5165719E-02	1.215819	+- 0.5673512E-02
295	1.204881	+- 0.5059210E-02	1.222242	+- 0.5172017E-02	1.226015	+- 0.5716288E-02
305	1.212285	+- 0.5072600E-02	1.209538	+- 0.5109848E-02	1.211155	+- 0.5636220E-02
315	1.200456	+- 0.5008944E-02	1.217581	+- 0.5129946E-02	1.213090	+- 0.5675053E-02
325	1.211473	+- 0.5081906E-02	1.211202	+- 0.5139041E-02	1.221121	+- 0.5708683E-02
335	1.208061	+- 0.5047382E-02	1.202971	+- 0.5116020E-02	1.221575	+- 0.5699175E-02
345	1.209278	+- 0.5057721E-02	1.212572	+- 0.5129397E-02	1.215215	+- 0.5675329E-02
355	1.211323	+- 0.5070264E-02	1.215256	+- 0.5159582E-02	1.213897	+- 0.5669750E-02

Table A2.8: Values of simulated muon charge ratio at different azimuth angles, with the zenith angles taken at intervals of 10° from 30° to 60° using the VENUS model.

Zenith angle 60° – 70°		70° – 80°		80° – 89°	
Azimuth (°)	Charge ratio	Charge ratio		Charge ratio	
5	1.199753	+- 0.7031033E-02	1.161202	+- 0.1081930E-01	0.925776	+- 0.2565851E-01
15	1.211560	+- 0.7107285E-02	1.168857	+- 0.1090903E-01	0.895735	+- 0.2488087E-01
25	1.205345	+- 0.7063303E-02	1.173665	+- 0.1096493E-01	0.985220	+- 0.2758162E-01
35	1.213914	+- 0.7133654E-02	1.167519	+- 0.1084407E-01	0.991075	+- 0.2767195E-01
45	1.216341	+- 0.7120804E-02	1.191170	+- 0.1114369E-01	1.022801	+- 0.2736414E-01
55	1.216408	+- 0.7056566E-02	1.211432	+- 0.1130121E-01	1.102025	+- 0.3003427E-01
65	1.208634	+- 0.7069054E-02	1.203810	+- 0.1118502E-01	1.181668	+- 0.3262534E-01
75	1.240489	+- 0.7302190E-02	1.220218	+- 0.1133925E-01	1.181964	+- 0.3215072E-01
85	1.229619	+- 0.7188624E-02	1.226177	+- 0.1152021E-01	1.210248	+- 0.3298211E-01
95	1.235597	+- 0.7253285E-02	1.258924	+- 0.1166536E-01	1.282174	+- 0.3566843E-01
105	1.237826	+- 0.7253297E-02	1.273684	+- 0.1179810E-01	1.401818	+- 0.3912051E-01
115	1.237547	+- 0.7246045E-02	1.296131	+- 0.1215818E-01	1.409850	+- 0.3865328E-01
125	1.245433	+- 0.7279891E-02	1.286061	+- 0.1194738E-01	1.595939	+- 0.4585876E-01
135	1.241770	+- 0.7284606E-02	1.308810	+- 0.1209773E-01	1.577275	+- 0.4424007E-01
145	1.245822	+- 0.7264744E-02	1.332736	+- 0.1243768E-01	1.726500	+- 0.4999896E-01
155	1.263220	+- 0.7390426E-02	1.350869	+- 0.1257809E-01	1.750131	+- 0.5031773E-01
165	1.266687	+- 0.7413524E-02	1.313015	+- 0.1231325E-01	1.807423	+- 0.5224494E-01
175	1.253036	+- 0.7342032E-02	1.346940	+- 0.1266078E-01	1.888388	+- 0.5544936E-01
185	1.254598	+- 0.7349642E-02	1.339207	+- 0.1252287E-01	1.740364	+- 0.5052842E-01
195	1.262234	+- 0.7414171E-02	1.349982	+- 0.1265125E-01	1.784465	+- 0.5055647E-01
205	1.233738	+- 0.7234625E-02	1.345342	+- 0.1269799E-01	1.761026	+- 0.4993451E-01
215	1.264748	+- 0.7413978E-02	1.328515	+- 0.1233330E-01	1.879444	+- 0.5483184E-01
225	1.246234	+- 0.7278567E-02	1.307495	+- 0.1220492E-01	1.686728	+- 0.4828212E-01
235	1.245731	+- 0.7306279E-02	1.307954	+- 0.1219684E-01	1.606630	+- 0.4552129E-01
245	1.232988	+- 0.7233135E-02	1.283959	+- 0.1203095E-01	1.451356	+- 0.4079307E-01
255	1.236465	+- 0.7253028E-02	1.258151	+- 0.1168891E-01	1.375445	+- 0.3812378E-01
265	1.240990	+- 0.7303640E-02	1.263203	+- 0.1170520E-01	1.254340	+- 0.3378737E-01
275	1.247219	+- 0.7370456E-02	1.214198	+- 0.1128733E-01	1.286188	+- 0.3492285E-01
285	1.220878	+- 0.7153017E-02	1.235778	+- 0.1156570E-01	1.128077	+- 0.3038620E-01
295	1.217512	+- 0.7170351E-02	1.197273	+- 0.1110277E-01	1.125591	+- 0.3069115E-01
305	1.224401	+- 0.7172528E-02	1.211221	+- 0.1127499E-01	1.062829	+- 0.2981116E-01
315	1.206540	+- 0.7051005E-02	1.170669	+- 0.1081195E-01	1.045347	+- 0.2903615E-01
325	1.208850	+- 0.7136403E-02	1.183751	+- 0.1095491E-01	1.007151	+- 0.2758300E-01
335	1.217611	+- 0.7141555E-02	1.144996	+- 0.1057233E-01	0.929213	+- 0.2537997E-01
345	1.204411	+- 0.7062717E-02	1.184040	+- 0.1103408E-01	0.912897	+- 0.2555023E-01
355	1.216715	+- 0.7155750E-02	1.158813	+- 0.1078761E-01	0.965159	+- 0.2651413E-01

Table A2.9: Values of simulated muon charge ratio at different azimuth angles, with the zenith angles taken at intervals of 10° from 60° to 89° using the VENUS model.